The pore domain outer helix contributes to both activation and inactivation of the hERG K+ channel

Pengchu Ju, Guilhem Pages, Peter Riek, Po-Chia Chen, Allan Torres, Paramjit Bansal, Serdar Kuyucak, Philip Kuchel, Jamie Vandenberg

THE JOURNAL OF BIOLOGICAL CHEMISTRY VOL. 284, NO. 2, pp. 1000–1008, January 9, 2009

The Pore Domain Outer Helix Contributes to Both Activation and Inactivation of the hERG K^+ Channel*[S]

Received for publication, August 19, 2008, and in revised form, October 10, 2008 Published, JBC Papers in Press, November 7, 2008, DOI 10.1074/jbc.M806400200

Pengchu Ju[‡§1], Guilhem Pages[¶1], R. Peter Riek[‡], Po-chia Chen[‖], Allan M. Torres[**], Paramjit S. Bansal[‡‡], Serdar Kuyucak[‖], Philip W. Kuchel[¶2], and Jamie I. Vandenberg[‡§¶3]

From the [‡]Division of Molecular Cardiology and Biophysics, Victor Chang Cardiac Research Institute, Darlinghurst, New South Wales 2010, Australia, [§]St. Vincent's Clinical School, University of New South Wales, Darlinghurst, New South Wales 2010, Australia, the [¶]School of Molecular and Microbial Biosciences, University of Sydney, New South Wales 2006, Australia, the [‖]School of Physics, University of Sydney, New South Wales 2006, Australia, the [**]School of Biomedical and Health Sciences, University of Western Sydney, New South Wales 1797, Australia, and the [‡‡]Australian Nuclear Science and Technology Organisation, PMB1, Menai, New South Wales 2234, Australia

Ion flow in many voltage-gated K^+ channels (VGK), including the (human *ether-a-go-go*-related gene) hERG channel, is regulated by reversible collapse of the selectivity filter. hERG channels, however, exhibit low sequence homology to other VGKs, particularly in the outer pore helix (S5) domain, and we hypothesize that this contributes to the unique activation and inactivation kinetics in hERG K^+ channels that are so important for cardiac electrical activity. The S5 domain in hERG identified by NMR spectroscopy closely corresponded to the segment predicted by bioinformatics analysis of 676 members of the VGK superfamily. Mutations to approximately every third residue, from Phe^{551} to Trp^{563}, affected steady state activation, whereas mutations to approximately every third residue on an adjacent face and spanning the entire S5 segment perturbed inactivation, suggesting that the whole span of S5 experiences a rearrangement associated with inactivation. We refined a homology model of the hERG pore domain using constraints from the mutagenesis data with residues affecting inactivation pointing in toward S6. In this model the three residues with maximum impact on activation (W563A, F559A, and F551A) face out toward the voltage sensor. In addition, the residues that when mutated to alanine, or from alanine to valine, that did not express (Ala^{561}, His^{562}, Ala^{565}, Trp^{568}, and Ile^{571}), all point toward the pore helix and contribute to close hydrophobic packing in this region of the channel.

There are dozens of different voltage-gated potassium channels (VGK)[4] in the human genome, and subtle differences in the regulation of the different VGKs underlie the diversity of neuronal activity and regional variations in the electrical activity of the heart (1). This diversity of function is reflected in the different clinical syndromes caused by mutations in VGKs (2). For example, mutations in the VGK encoded by hERG (human *ether-a-go-go*-related gene) (3, 4) or channel block by a wide range of prescribed medications (5) prolong ventricular action potentials and greatly increase the risk of cardiac arrhythmia and sudden death (6). Elucidating the pathophysiology of such clinical syndromes requires an application of knowledge of the fundamental mechanisms of how ion channels work (7–9) coupled to a detailed investigation of the subtleties of the regulation of each of the individual ion channels concerned.

VGKs assemble as tetramers with each subunit containing six transmembrane domains (denoted S1–S6; see Fig. 1). The S5 and S6 domains along with the intervening pore loop from each of the four subunits form the pore domain (1). The pore loop also contains the selectivity filter (10). In many K^+ channels, including the archetypal bacterial K^+ channel, KcsA (11, 12), the classical VGK, Shaker (13), and hERG K^+ channel (14, 15), reversible collapse of the selectivity filter serves an important role in gating ion flow via so-called C-type inactivation. In KcsA and Shaker, the selectivity filter is supported by a hydrogen bond network (7, 10) and cradled by surrounding transmembrane helices (10). However, in the pore domain region, hERG exhibits low sequence homology to other members of the superfamily of VGKs. For example, the residues involved in the hydrogen bond networks around the selectivity filter in KcsA and Shaker are not conserved in hERG, and there is a particularly low sequence homology in the outer pore helix domain (S5) (16). In VGKs, the outer pore domain helix (S5) also serves as an interface with the voltage sensor domains (S1–S4) and thereby contributes to regulating the activation properties of the channel. We therefore hypothesized that the outer pore helix of the hERG K^+ channel may contribute to the differences

* This work was supported by Project Grant 459002 from the National Health and Medical Research Council (to J. I. V. and S. K.) and Project Grant DP0450808 from the Australian Research Council (to P. W. K. and J. I. V.). The costs of publication of this article were defrayed in part by the payment of page charges. This article must therefore be hereby marked "*advertisement*" in accordance with 18 U.S.C. Section 1734 solely to indicate this fact.

[S] The on-line version of this article (available at http://www.jbc.org) contains supplemental Tables S1 and S2 and Figs. S1 and S2.

[1] These authors contributed equally to this work.

[2] Recipient of Australian Research Council Australian Professorial Fellowship DP0345961.

[3] Recipient of National Health and Medical Research Council Senior Research Fellowship 459001. To whom correspondence should be addressed: Mark Cowley Lidwill Research Program in Cardiac Electrophysiology, Victor Chang Cardiac Research Institute, 405 Liverpool St., Darlinghurst, NSW 2010, Australia. Tel.: 61-2-9295-8771; Fax: 61-2-9295-8770; E-mail: j.vandenberg@victorchang.edu.au.

[4] The abbreviations used are: VGK, voltage-gated potassium channel; CNG, cyclic nucleotide gated; DPC, dodecyl phosphocholine; GES, Goldman-Engelman-Steitz; HCN, hyperpolarization activation channel; WT, wild type; HBTU, 2-(1H-benzotriazol-1-yl)-1,1,3,3-tetramethyluronium hexafluorophosphate; NOESY, nuclear Overhauser enhancement spectroscopy.

in inactivation and activation properties of these channels compared with other members of the VGK family. Accordingly, the aims of this study were to identify the transmembrane extent of the outer pore helix and investigate to what extent mutations in the outer pore helix affected steady state activation and inactivation properties of the channel.

MATERIALS AND METHODS

Bioinformatics—An alignment table containing all available members of the canonical VGK, (*ether-a-go-go*) EAG, hyperpolarization activated (HCN), and cyclic nucleotide gated (CNG) families was built. The initial alignment was based on a clustal alignment (17) of the human sequences with no gaps for the S5 segments. All available additional canonical VGK, EAG, HCN, and CNG sequences were added and aligned manually to the initial alignments. To remove bias, caused by there being different numbers of sequences for each different subtype within each subfamily, each group of subtype sequences (defined as proteins with >95% sequence similarity) was reduced to the equivalent of one sequence, *i.e.* the sum of the proportions of each amino acid type at each position equaled one. Absolutely conserved positions had a single amino acid type given a value of one, whereas less conserved positions had a variety of amino acids each with a value of less than one that was proportional to their frequency. The overall distribution of amino acids at each position within the entire family or subfamily was determined by summing the individual amino acid proportions for each channel subtype and dividing by the number of subtypes.

The degree of conservation of relative hydrophobicity was calculated as described in Riek *et al.* (18). Similarity matrices were built using the Goldman-Engelman-Steitz (GES) hydrophobicity scale (19) or the ΔG_{app} hydrophobicity scale (20). At each position, each amino acid was compared with all other amino acids at that position, and the degree of similarity was summed, divided by the number of amino acid pairs, and plotted. Diagrams summarizing the conservation of residues at each position were generated using a custom written software package developed by one of us (R. P. Riek) and implemented on a SGI platform.

Peptide Synthesis—The 43-residue hERG S5 peptide was synthesized on a 0.50-mmol scale using HBTU activation of Boc-amino acids with *in situ* neutralization chemistry, as previously described (21). Boc-L-amino acids were obtained from Novabiochem (Laufelfingen, Switzerland) or Peptide Institute (Osaka, Japan). HBTU was obtained from Richelieu Biotechnologies (Quebec, Canada). Trifluoroacetic acid, *N,N*-diisopropylethylamine, and *N,N*-dimethylformamide, all peptide synthesis grade, were purchased from Auspep (Melbourne, Australia). All other chemicals were of analytical grade from commercial suppliers.

The peptide was assembled manually by stepwise solid phase synthesis using an *in situ* neutralization protocol for Boc chemistry (22). Starting from Boc-Tyr(2BrZ)-OCH2-Pam resin (0.25 mmol, loading 0.753 mmol/g), 1 mmol of Boc protected amino acids were coupled using HBTU and excess *N,N*-diisopropylethylamine as activating agent. The side chain protecting groups were: Arg(Tos), Asp(OcHxl), Cys(MeBzl), Glu (OcHxl), His(DNP), Lys(2-ClZ), Ser(Bzl), Thr(Bzl), Trp(CHO), and Tyr(2-BrZ). Following assembly the peptide was cleaved from the resin, and side chains were simultaneously deprotected, by treatment with anhydrous hydrofluoric acid: *p*-cresol: *p*-thiocresol (9: 0.5: 0.5, v/v, −2 °C, 90 min). The crude products were precipitated with cold diethyl ether, then extracted into 50% aqueous acetonitrile containing 0.05% trifluoroacetic acid, and lyophilized.

Purification was achieved by semi-preparative reverse phase high pressure liquid chromatography (Vydac C4 column, 10 × 250 mm) using a linear gradient of 0–90% acetonitrile in water and 0.1% trifluoroacetic acid over 50 min at a flow rate of 3 ml/min. The purified peptide was used for further studies. Mass spectra were recorded on a QSTAR XL mass spectrometer equipped with a matrix-assisted laser desorption ionization source (Applied Biosystems Inc., Foster City, CA). Mass spectra were obtained over the range m/z 800–2000 with a step size of 0.2 Da. Data acquisition and processing were done using analyst software.

NMR Spectroscopy—The NMR spectroscopy sample consisted of 1.8 mM (3.2 mg) of S5 peptide dissolved in 350 μl of 90/10, H_2O/D_2O, v/v containing 107 mM (14.6 mg) of deuterated dodecylphosphocholine (DPC; Cambridge Isotope Laboratories, Andover, MA). The paramagnetic relaxation agent gadolinium-diethylenetriamine pentaacetic acid-bismethylamide (a gift from Dr. Klaus Zangger, University of Graz, Graz, Austria) was introduced to this sample at a concentration of 2.3 mM (0.5 mg).

All of the experiments were performed on a Bruker Avance-600 DRX spectrometer (Karlsruhe, Germany) equipped with a 5-mm triple resonance inverse cryoprobe with sample temperatures of 25, 30, and 35 °C. The two-dimensional experiments performed were total correlation spectroscopy (23) with Malcolm Levitt's composite-pulse decoupling sequence (MLEV) spin-lock of 60 or 90 ms and nuclear Overhauser enhancement spectroscopy (NOESY) (24) with mixing time of 300 ms. All two-dimensional experiments were acquired using time-proportional phase detection (25). A WATERGATE pulse sequence (26) was used to achieve water signal suppression. Two identical NOESY experiments were performed at 35 °C before and after the addition of the paramagnetic relaxation agent to compare signal intensities. All of the spectra were processed on XWINNMR v3.2 software (Bruker) and were analyzed using the program XEASY (27).

Residue assignments were made according to the standard protocol from all total correlation spectroscopy and NOESY experiments. To analyze the effect of the relaxation agent gadolinium-diethylenetriamine pentaacetic acid-bismethylamide, rectangles were drawn around each labeled peak in the NOESY experiments, recorded before and after the addition of gadolinium, and integration of cross-peaks was performed for all rectangles using the same contour plot level.

Molecular Biology—HERG cDNA (kindly supplied by Dr. Gail Robertson, University of Wisconsin) was subcloned into a pBluescript vector containing the 5′-untranslated region and 3′-untranslated region of the *Xenopus laevis* β-globin gene (a gift from Dr. Robert Vandenberg, University of Sydney). Residues 543–577 were singly mutated to Ala (or from Ala to Val). Conservative mutations were made to residues where Ala/Val substitution was not tolerated or resulted in markedly abnormal function.

Mutagenesis was carried out using the megaprimer PCR method as previously described in detail (28). Mutant constructs were confirmed by bi-directional sequencing. Wild type and mutant channel cDNAs were linearized with BamHI and cRNA transcribed with T7 RNA polymerase using the mMessage mMachine kit (Ambion, Austin, TX).

Electrophysiology—X. laevis oocytes were prepared as previously described (29). All of the experiments were approved by the University of Sydney Animal Ethics Committee. The oocytes were injected with 5–10 ng cRNA and incubated at 18 °C for 24–72 h prior to electrophysiological recordings. All experiments were carried out at room temperature (21–22 °C). Two-electrode, voltage-clamp experiments were performed using a Geneclamp 500B amplifier (Molecular Devices, Sunnyvale, CA). Glass microelectrodes had tip resistances of 0.3–1.0 MΩ when filled with 3 M KCl. The bath solution was 96 mM NaCl, 2 mM KCl, 1 mM $MgCl_2$, 1 mM $CaCl_2$, and 10 mM HEPES (pH 7.6). Data acquisition and analysis were performed using pCLAMP 9.2 (Molecular Devices) and Excel software (Microsoft, Seattle, WA). All data are shown as means ± S.E. Measurements of steady state activation and inactivation were performed as previously described (28, 30). Steady state activation and inactivation data were analyzed using a simple two-state Boltzmann function,

$$g/g_{max} = [1 + \exp((\Delta G_0 - z_g EF)/RT)]^{-1} \quad \text{(Eq. 1)}$$

where ΔG_0 is the difference in Gibbs' free energy between states at 0 mV, z_g is the effective number of electric charges crossing the transmembrane electric field, F is the Faraday constant, R is the universal gas constant, and T is the absolute temperature. For mutations that cause perturbations in ΔG_0 for activation or inactivation, we conclude that the residue involved changes its environment during the activation or inactivation process. It is important to note, however, that because these are steady state measurements we cannot determine when or how this change in environment takes place. Perturbations in ΔG_0 are quantified as follows,

$$\Delta\Delta G_0 = \Delta G_{0,Mut} - \Delta G_{0,WT} \quad \text{(Eq. 2)}$$

where $\Delta\Delta G_0$ is the difference in the changes in Gibbs' free energy between the mutant ($\Delta G_{0,Mut}$) and WT ($\Delta G_{0,WT}$). Typically, cut-off values for significant differences have used a value of ± 1 kCal mol^{-1} (31, 32), and we have used this cut-off for perturbations to steady state activation. Mutation-induced shifts in the ΔG_0 of inactivation, however, tend to be much smaller than for activation because of the less steep voltage dependence of inactivation compared with activation (supplemental Table S2). For this reason, previous investigators (32) have used a smaller cut-off value of $\Delta\Delta G_0 > \pm 0.5$ kcal mol^{-1} to indicate significant perturbations to steady state inactivation. We have also used this lower cut-off for our inactivation studies.

Structural Modeling—The simulation systems for the channel models were constructed using the VMD suite of software (33). Molecular dynamics simulations were carried out using NAMD code version 2.6 (34) and the CHARMM27 force field (35) with the CMAP correction for the dihedral terms included (36).

The initial model coordinates for the hERG pore domain were extracted from the open state model supplied by Dr. H. R. Guy (National Institutes of Health) (37). To produce a closed state, the kink in S5 was manually removed, and the residues Ala^{653}, Gly^{657}, and Ser^{660}, located in the neighborhood of Phe^{656}, were selected for constriction via the application of harmonic forces. The channel was deemed closed when the Phe^{656} side chains from each monomer came into van der Waals' contact. The model of Tseng *et al.* (37) includes proposed coordinates for the "turret region" between the end of S5 and start of the pore helix, *i.e.* the S5P linker. Because there are no experimental data on the three-dimensional structure of this region, the backbone atoms from residues 575 to 602 were restrained, so as to prevent turret mobility from interfering with the rest of the channel. This restriction applies to all simulations conducted in this study.

Modifications were introduced to bring this model into conformity with other K^+ channel crystal structures, aiming to reproduce the location of conserved residues. This required small rotations and translations of the S5 and S6 helices. Clashes introduced during this process were resolved by further side chain rotations. The open and closed state models thus obtained were embedded in a lipid bilayer consisting of 1-palmitoyl-2-oleoyl-phosphatidylethanolamine molecules and solvated with a 100 mM KCl solution. Each system was gradually relaxed over 500 ps of molecular dynamics simulations. First the harmonic restraints on the side chains were relaxed over 250 ps in 50-ps steps while the backbone was fixed. Then the restraints on the backbone atoms were relaxed in a similar manner over 250 ps. Unconstrained simulations (with the exception of the turret region noted above) were then carried out for 2.5 ns to confirm the stability of the models.

RESULTS

Identification of the hERG S5 Segment—Based on the conservation of hydrophobicity in 676 sequences (115 groups) of members of the VGK channel superfamily, we predicted that the likely transmembrane region of the hERG S5 segment would span L550-A570 (Fig. 1*C*). Unlike the pore helix (10) and S6 domains (38), there are no highly conserved residues in the S5 domain. The most highly conserved residue being an aromatic residue at the 19^{th} position of the putative transmembrane domain (63.4% tyrosine, 15.5% tryptophan, 9.1% phenylalanine; Trp^{568} in hERG; Fig. 1, *C* and *D*) and a leucine at the third residue of the putative transmembrane domain in 65.5% of sequences, that is also present in hERG; Leu^{552}. A detailed analysis of the distribution of amino acids at each position is shown in supplemental Fig. S1. Splitting the channels into the three major subgroups: the canonical VGK (*e.g.* Shaker), EAG, and CNG + HCN families, revealed much higher homology for the S5 segment between the EAG and CNG + HCN families than for either of these to the canonical VGK family (Fig. 1, *D* and *E*).

To investigate more directly the structure and extent of the S5 domain in hERG, we used NMR spectroscopy to study a

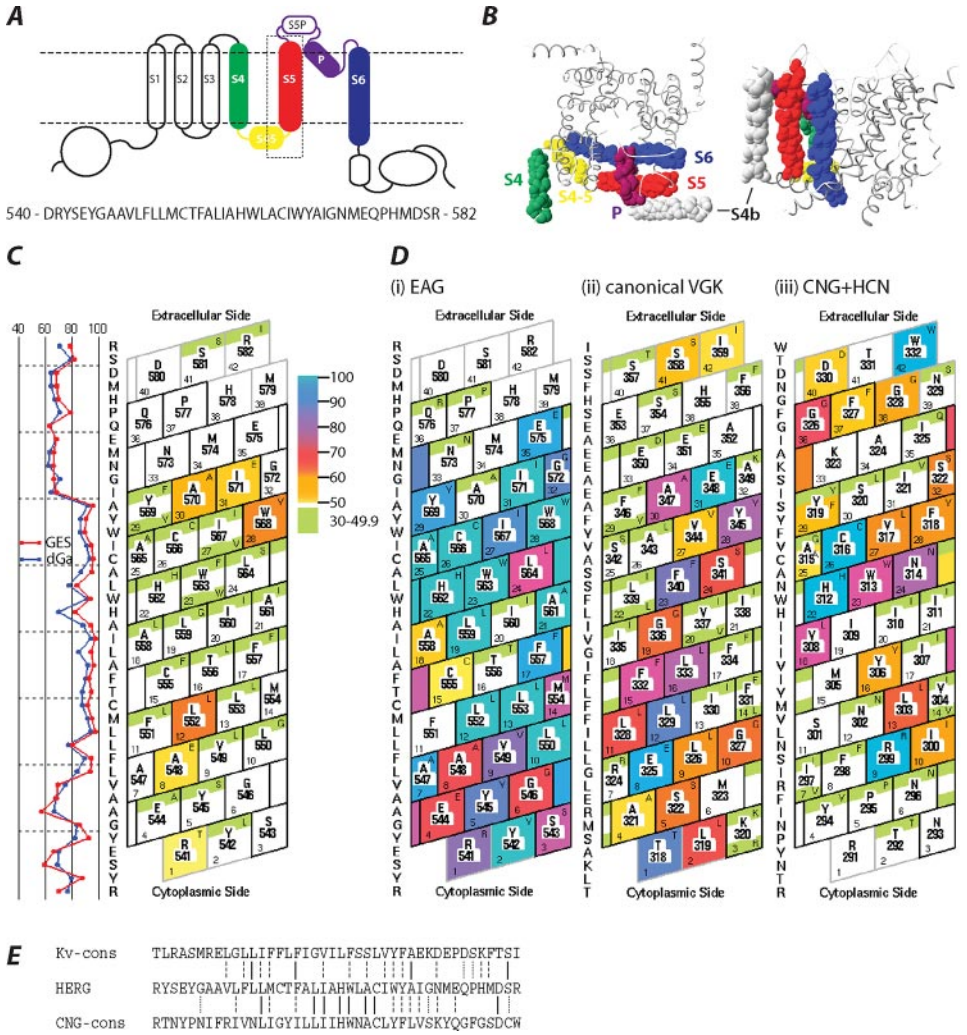

FIGURE 1. **Topology of hERG channels and alignment of sequence being analyzed with related ion channels.** *A*, topology of a single hERG subunit, colored as per *B*. The *dotted box* highlights the region of the channel (Asp^{540}–Arg^{582}) investigated in this study. *B*, x-ray structure of the pore domain and S4 segment of Kv12 shown from the *top* and *side views*. The S4 helix (*green*), S4-S5 helix (*yellow*), S5 helix (*red*), pore helix (*purple*), and S6 helix (*blue*) from one subunit are highlighted in space fill representation. The S4 segment from the adjacent subunit is highlighted in *gray*. *C*, sequence conservation for 676 members of the VGK superfamily. The helical net diagrams represent each position as a rhomboid with 3.6 residues per turn. The sequence shown is that for hERG, and the color coding indicates the degree of sequence identity at each position. The most frequent residue at each position is shown in the *top right corner* of each rhomboid. The complete table for all sequences is shown in supplemental Fig. S1 on-line. The conservation of hydrophobicity, according to the Goldman-Engelman-Steitz (*red*) or dGA (*blue*) scales, are plotted to the *left*. *D*, helical net diagrams showing sequence conservation within (*panel i*) EAG family, (*panel ii*) canonical VGK family, and (*panel iii*) CNG + HCN families. The color scheme is as for *C*. The sequences shown in each panel are that for (*panel i*) hERG (GenBank™ accession number Q12809), (*panel ii*) rat Kv12 (GenBank™ accession number NP_775118), and (*panel iii*) mouse HCN2 (GenBank™ accession number NP_032252). *E*, sequence alignment using ClustalW (17) for hERG, the consensus sequence for the canonical VGKs, and the consensus CNG + HCN sequence. The *solid lines* indicate identity, *dashed lines* indicate strong homology, and *dotted lines* indicate moderate homology.

43-residue synthetic peptide corresponding to Asp^{540}–Arg^{582}, *i.e.* a region that extended well beyond the predicted N- and C-terminal limits of S5 (Fig. 1).

The Asp^{540}–Arg^{582} peptide had limited solubility in aqueous media but could be reconstituted in DPC micelles. The high helical structure of the peptide resulted in considerable spectral overlap in the aliphatic region of the spectrum and prevented determination of its high resolution structure (Fig. 2*A*). However, combining chemical shift indices and signal attenuation caused by the paramagnetic relaxation reagent Gd^{3+}, qualitative information was extracted.

The consecutive negative values of the Cα ^{1}H chemical shift index confirmed that the peptide adopted a predominantly helical conformation (Fig. 2*B*). The chemical shift index plots suggest the presence of helical domains in Tyr^{545}–Val^{549}, Phe^{551}–Ala^{570}, and Gly^{572}–Pro^{577}. The central helical element is consistent with that predicted from the bioinformatics analysis discussed above (Fig. 1, *C* and *D*). The additional helical segments suggest that the helical segment for S5 may extend beyond the hydrophobic interior of the DPC micelles and into the extramicellar solution. To investigate this possibility, we incubated the DPC-peptide micelles with Gd^{3+}, a paramagnetic relaxation reagent that suppresses signals from the extramicellar environment (39, 40). Gd^{3+} caused very little suppression of any signals from the central region of the peptide (Phe^{551}–Ala^{570}), consistent with the putative location of this segment within the micelles. Conversely, Gd^{3+} caused marked suppression of almost all of the remaining signals (Fig. 2*C*). This suggested that the remainder of the peptide was indeed extramicellar. Two notable exceptions to this pattern were the residues equivalent to Tyr^{545} and Val^{549} that were not suppressed by Gd^{3+}, suggesting that they point into the micelle. Additionally, the side chain for Ile^{571} was not suppressed by Gd^{3+}, suggesting that it also points into the micelle.

Together, the bioinformatics and NMR data suggest that the S5 domain of hERG is helical, it begins at Phe^{551} and extends to Ala^{570}. This domain is preceded by a helix that lies parallel to the plasma membrane with Tyr^{545} and Val^{549} pointing toward the micelle, consistent with the location of the S4-S5 helix seen in the Kv12 crystal structure (Fig. 1*B*), and at the extracellular end there is a helical segment that extends into the extracellular solution. A cartoon depicting these structural features is shown in Fig. 2*D*.

Mutations to Residues in S5 Perturb Activation and Inactivation—To investigate the functional role of S5 in hERG, residues from Ser^{543} to Pro^{577} were individually mutated to alanine or from alanine to valine. Five of the mutant channels were nonfunctional (A561V, H562A, A565V, W568A, and Q576A) and two expressed poorly (F557A and I571A). More

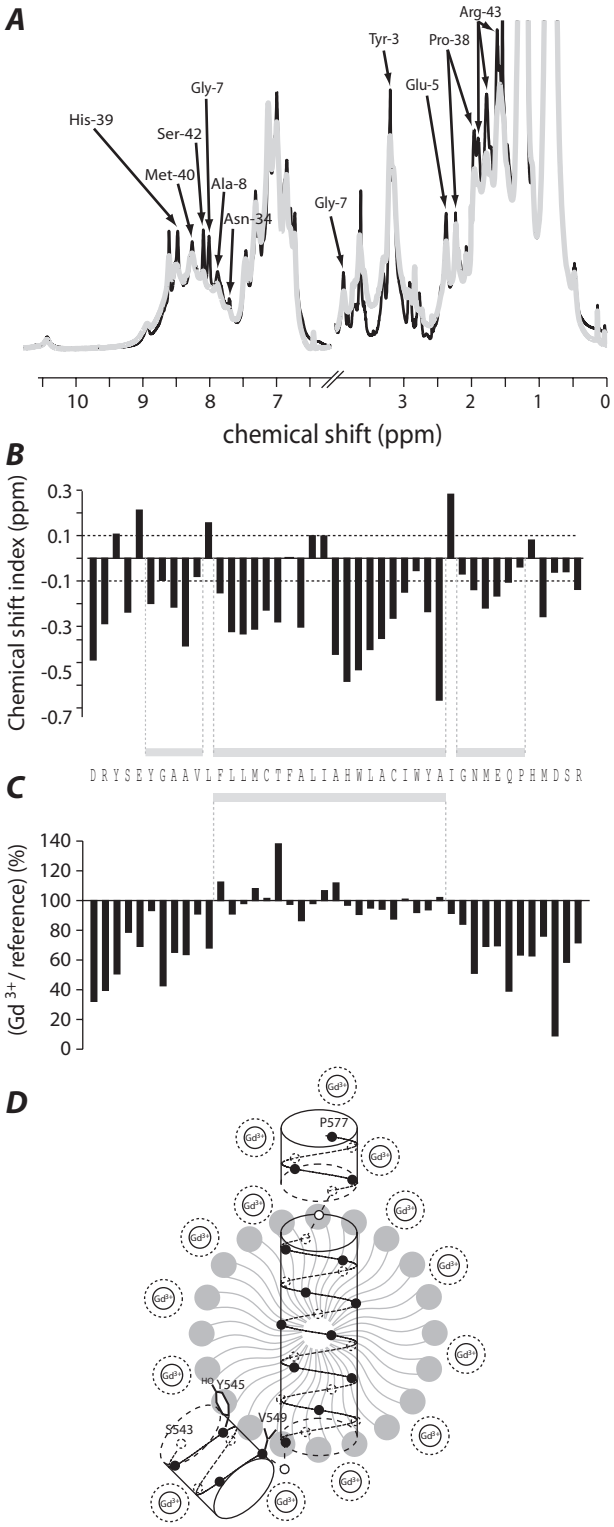

FIGURE 2. **NMR spectroscopy analysis of the S5 peptide in micelles.** *A*, ^{1}H NMR spectra of S5 peptide in DPC micelles in the presence (*gray*) and absence (*black*) of Gd^{3+}. Gd^{3+} resulted in significant attenuation of the signal intensity of approximately half the peaks (labeled peaks), whereas the other peaks were slightly or not affected. *B*, chemical shift index plot for the Cα ^{1}H resonances of the S5 peptide in DPC micelles. A stretch of four or more negative values not interrupted by any residues with a chemical shift index value < 0.1 is indicative of an α-helix. The *gray bars* indicate predicted stretches of α-helix. *C*, percentage suppression of peaks by Gd^{3+}. The *gray bar* indicates the stretch of residues (Phe^{551}–Ala^{570}) where there is minimal suppression of signals by Gd^{3+}. *D*, cartoon depicting the putative structure of the S5 segment including an S4-S5 helix lying parallel to the surface of the micelle with residues Tyr^{545} and Val^{549} pointing into the micelle, a transmembrane segment from Phe^{551} to Ala^{570} and an extracellular helical segment stretching from Gly^{572} to Pro^{577}. The sinusoidal lines superimposed on the helices are coded to indicate whether they are on the front of the helix (*solid line*) or back of the helix (*dashed lines*). Similarly residue locations on the front of the helix are shown in *solid circles*, and residues on the back of the helix are shown in *dashed open circles*.

conservative mutations were constructed for these residues (A561C, H562N/T, A565C, W568F, Q576N, F557L, and I571L).

Mutants That Affect Steady State Activation Are Restricted to the Inner Two-thirds of the S5 Domain and the S4-S5 Linker—Typical examples of current traces recorded from oocytes expressing WT or W563A mutant hERG channels in response to 4-s depolarization steps in the voltage range −100 to +40 mV are illustrated in Fig. 3*A*. W563A resulted in an ~30-mV leftward shift in the voltage dependence of channel activation (Fig. 3*B*) that corresponded to a change in the free energy of activation, $\Delta\Delta G_0$, of -3.2 ± 0.15 kcal mol^{-1} ($n = 3$). The changes in $\Delta\Delta G_0$ of activation for functional mutants are summarized in Fig. 3*C*, and the values for the midpoint and slope factor of the voltage dependence of activation are summarized in supplemental Table S1.

Trp^{563}, located in the mid portion of the putative transmembrane domain, is the most C-terminally located residue in the region studied that when mutated resulted in a significant perturbation to steady state activation (Fig. 3*C*). Mutations to residues Leu^{559}, Phe^{557}, Thr^{556}, and Phe^{551} also resulted in significant perturbations to steady state activation. In addition to the residues within the putative transmembrane region, all of the residues in the S4-S5 linker region (Ser^{543}–Val^{549}) caused significant perturbations to the voltage dependence of steady state activation (Fig. 3*C*).

Mutants That Affect Steady State Inactivation Are Distributed throughout the S5 Domain and Extracellular Extension—Typical examples of current traces recorded from oocytes expressing WT or L564A mutant hERG channels in response to a two-step voltage protocol designed to measure steady state inactivation (30) are illustrated in Fig. 4*A*. L564A resulted in an ~70-mV rightward shift in the voltage dependence of channel availability (Fig. 4*B*) that corresponded to a change in the free energy of inactivation, $\Delta\Delta G_0 = 1.5 \pm 0.14$ kcal mol^{-1} ($n = 4$). Note that larger voltage shifts in the midpoint of steady state inactivation compared with steady state activation curves (*e.g.* compare Figs. 3*B* and 4*B*) resulted in smaller values of $\Delta\Delta G_0$ for steady state inactivation (compare Figs. 3*C* and 4*C*) because of the less steep voltage dependence of inactivation compared with activation (supplemental Table S2). For this reason, previous investigators (32) have used a smaller cut-off value of $\Delta\Delta G_0 > \pm 0.5$ kcal mol^{-1} to indicate significant perturbations to steady state inactivation. We therefore used this same lower cut-off.

The mutations that resulted in a significant perturbation to steady state inactivation, based on a 0.5 kcal mol^{-1} cut-off, are distributed throughout the putative transmembrane domain (Fig. 4*C*). In addition to the residues within the putative transmembrane region, residues in the extracellular extension (Asn^{573}, Glu^{575}, and Pro^{577}) and Tyr^{545} in the S4-S5 linker

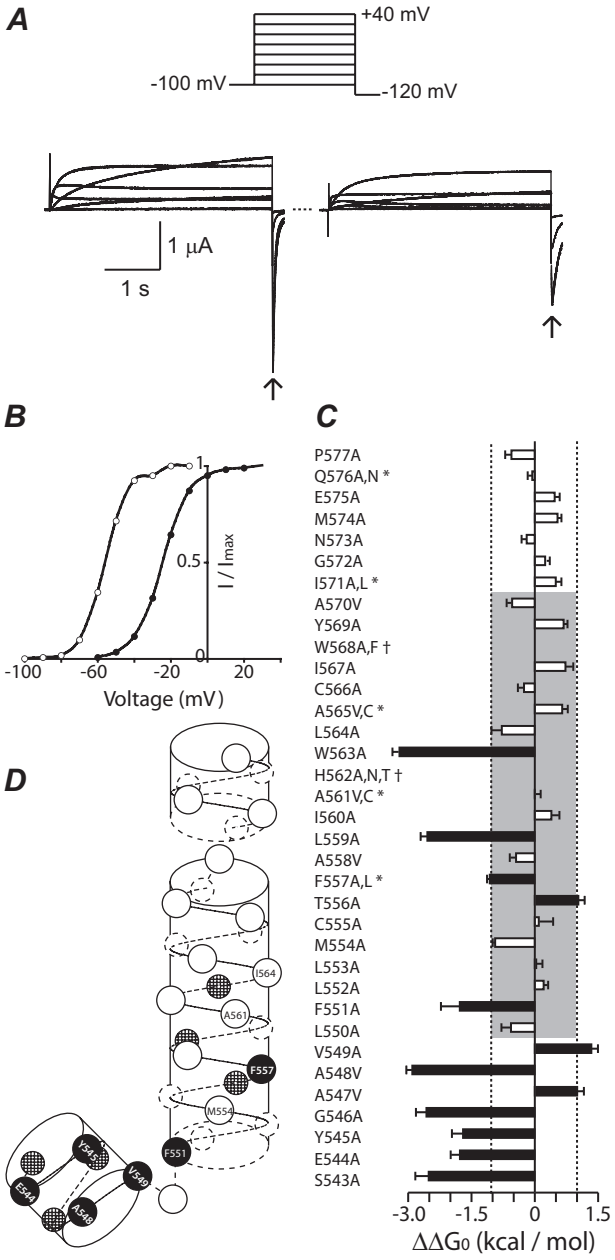

FIGURE 3. **Effects of Ala substitutions on the voltage dependence of steady state activation.** *A*, typical examples of currents recorded from WT and W563A mutant hERG channels during 4-s isochronal activation protocols (voltage protocol shown at *top* of panel). *Arrows* indicate where peak tail currents were measured for calculation of steady state activation parameters (see *B*). *B*, steady state activation curves corresponding to the WT hERG (*filled circles*) and W563A (*open circles*) from current traces illustrated in *A*. *C*, bar graph plot of $\Delta\Delta G_{0,act}$ against primary amino acid position. The *filled bars* indicate mutations that caused >1 kcal mol^{-1} shift in $\Delta\Delta G_{0,act}$ (*gray shaded area*). *, A561V, A565V, I571A, and Q576A expressed very poorly but A561C, A565C, I571L, and Q576N did express, and it is the data for the later mutants that are shown. †, W568A/F and H562A/N/T failed to express or currents were too low to measure parameters for steady state activation. *D*, mapping of residues causing a perturbation to activation onto the cartoon depiction of the S5 peptide in DPC micelles (see Fig. 2*D*). Residues on the front of the helix that perturbed activation are shown as *solid circles* and labeled, and residues on the back of the helix that perturbed activation are shown in *hashed shading*.

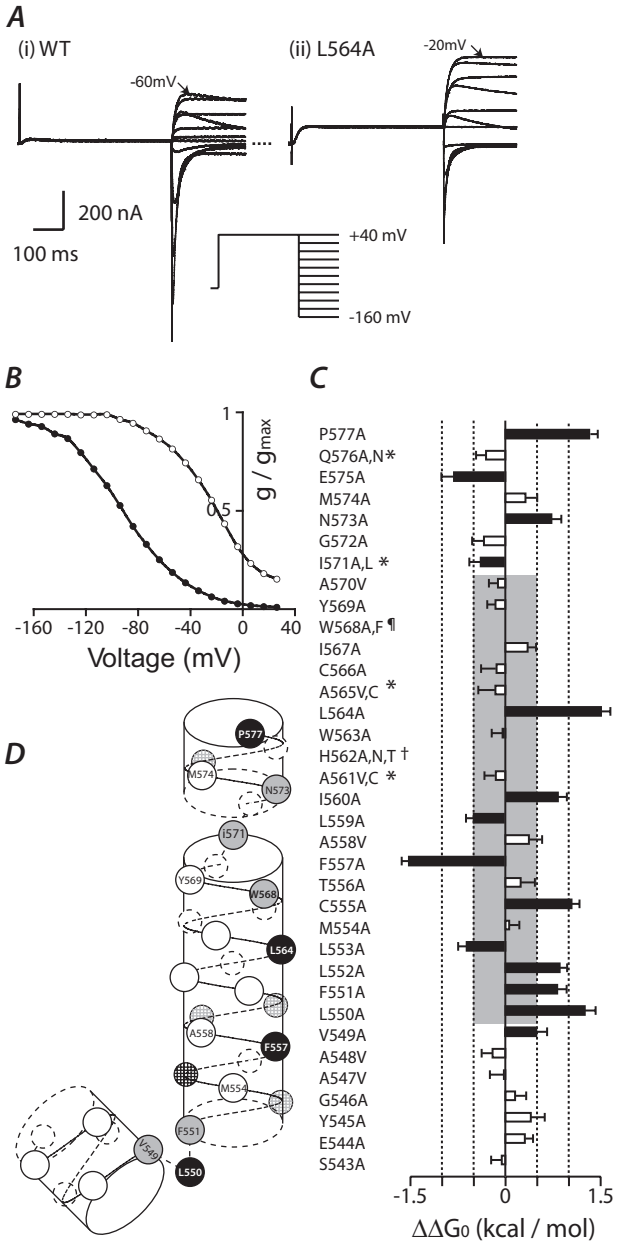

FIGURE 4. **Effects of Ala substitutions on the voltage dependence of steady state inactivation.** *A*, typical example of current traces recorded from WT and L564A hERG channels during a two-step voltage protocol (shown at top of WT hERG current traces) to measure steady state inactivation. *B*, conductance-voltage relationships of steady state inactivation for the current traces shown in *A*. *Filled circles*, WT hERG; *open symbols*, L564A hERG channels. *C*, bar graph plot of $\Delta\Delta G_{0,inact}$ against primary amino acid position. *, A561V, A565V, I571A, and Q576A expressed very poorly, but A561C, A565C, I571L, and Q576N did express, and it is the data for these mutants that are shown. †, H562A,N,T failed to express. ¶ W568A failed to express and W568F gave very small expression but had left shifted steady state inactivation. A cut-off value of >±0.5 kcal mol^{-1} (*gray shaded area*) was used for significant perturbations, as previously described (32). *D*, mapping of residues causing a perturbation to inactivation onto the cartoon depiction of the S5 peptide in DPC micelles (see Fig. 2*D*). *Black* indicates perturbation of >±1 kcal mol^{-1}, and *gray* indicates perturbation of >±0.5 kcal mol^{-1} or residues that when mutated to Ala were nonexpressing but when mutated to a more conservative mutation affected steady state inactivation. The *filled symbols* indicate residues on the front of the helix, and the *hashed symbols* are on residues on the back of the helix.

region caused significant perturbations to steady state inactivation (Fig. 4*C*). The residues within the putative transmembrane domain that affect steady state inactivation line up predominantly on one face of the helix (Fig. 4*D*). This face is rotated ~120° from the face of the helix affecting steady state activation (compare Figs. 4*D* and 3*D*).

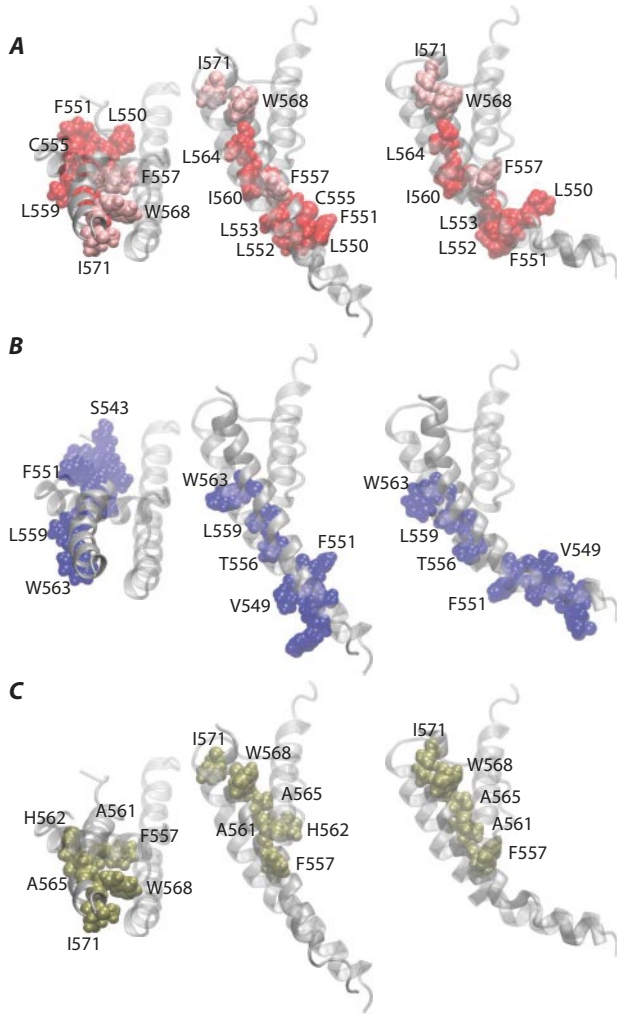

FIGURE 5. **Homology model of the hERG pore domain.** Views of the homology model shown from the top (closed state) and from the side (closed and open states). The model was constrained so that residues that perturb inactivation when mutated to alanine (or more conservative mutations, see Fig. 4), highlighted in *red*, point toward S6 (*A*). As a consequence, residues that perturbed activation when mutated to alanine (see Fig. 3), highlighted in *blue*, point away from the pore (*B*), and residues where mutations to alanine or from alanine to valine did not express (highlighted in *olive*) point toward the pore helix (*C*).

Homology Model of the hERG Pore Domain—The results from the mutagenesis data in this study were mapped onto a homology model of the hERG pore region (Fig. 5). Residues that affected steady state inactivation when mutated were found to face S6, a pattern that was used to further refine the model to optimize these contacts. This orientation of S5 also predicted that: first, residues affecting steady state activation faced outwards toward the voltage sensor domain, and second, the nonexpressing mutants, *i.e.* residues that when mutated to alanine, or from alanine to valine, did not express (Ala^{561}, His^{562}, Ala^{565}, Trp^{568}, and Ile^{571}), all pointed toward the pore helix and contribute to close hydrophobic packing in this region of the channel (Fig. 5*C*). This latter result is consistent with data obtained for Shaker channels (41) where mutations that were nonfunctional faced toward the pore helix.

DISCUSSION

Extent of S5 Domain—NMR spectroscopy analysis of an isolated peptide, spanning the S5 domain of hERG, suggests that the transmembrane domain of S5 corresponds to Phe^{551}–Ala^{570}. Given recent studies suggesting that specific lipid groups can exert an important influence on ion channel structure (8, 42, 43), it is important to consider whether the structure deduced from our studies with DPC micelles accurately reflect the structure of the S5 domain in the intact channel in cell membranes. Independent evidence in favor of the central hydrophobic core identified in our micelle studies being the transmembrane domain include first, the bioinformatics analysis of 676 K^+ channel sequences from 115 sequence groups indicating a conserved hydrophobic core that spans the residues that are equivalent to Leu^{550}–Ala^{570} (Fig. 1). Second, from the analysis of perturbations to inactivation, the first residue to have a large perturbation to the voltage dependence of steady state inactivation was Leu^{550}, and from this position every third or fourth residue also perturbed inactivation (Leu^{550}, Leu^{553}, Phe^{557}, Ile^{560}, and Leu^{564}) finishing with Ile^{571} that when mutated to alanine did not express and when mutated to the very similar Leu caused a modest shift in inactivation (Fig. 4). In addition, Trp^{568} when mutated to alanine did not express and when mutated to phenylalanine expressed only poorly but showed a perturbation to inactivation (data not shown).

The second significant feature of the NMR analysis is the presence of a helical element at the N terminus of the peptide. This probably corresponds to a portion of the helix in the S4-S5 linker region, as is seen in the crystal structures of Kv12 (8). The observations that both Tyr^{545} and Val^{549} are protected from signal suppression by Gd^{3+} (Fig. 2*C*) suggests that the S4-S5 helix must lie parallel to the micelle surface (Fig. 2*D*), an observation that is also consistent with the location of the S4-S5 linker in the crystal structure (8). Every residue in the S4-S5 helical region (Ser^{543}–Val^{549}) perturbed activation, a finding that is consistent with previous studies showing that the S4-S5 linker is important in coupling movement of the voltage sensor to movement of the activation gate at the cytoplasmic end of S6 (44).

Thus both the bioinformatics and electrophysiology results in this study, in conjunction with previous crystallography studies of related K^+ channels (8, 45), support the notion that the structure deduced from the current NMR experiments closely resembles the structure of the S5 domain of the intact channel under native conditions. However, we cannot exclude the possibility that the boundaries between the S4-S5 linker and the transmembrane S5 domain and between the transmembrane S5 domain and the extracellular region may vary by one or two residues.

Effect of S5 Mutations on Steady State Activation—The residues that had the greatest impact on activation, when mutated to alanine, were Trp^{563}, Leu^{559}, and Phe^{551} with Thr^{556} and Phe^{557} having a moderate impact (Fig. 3). These residues are located in the C-terminal half of the transmembrane segment and roughly cover one face of the predicted S5 helix. Of these residues, only Trp^{563} and Leu^{559} are 100% conserved in the EAG subfamily, and these residues are moderately conserved in the CNG/HCN family but not conserved in the canonical VGK family (see supplemental Figs. S1 and S2). The reasonably high conservation between CNG/HCN and EAG families suggests that the interaction between the S5 domain and the voltage

sensor domain may be conserved between these subfamilies. Conversely, the interaction between these two domains is likely to differ between the canonical Kv and EAG families. Alanine and tryptophan (41, 46) scanning mutagenesis studies on Shaker are consistent with this hypothesis. Specifically, there appear to be two hotspots on the Shaker S5 segment that are important for interaction with the VSD, a segment in the intracellular half of the S5 domain (41), similar to that observed here for hERG, and an additional hot spot at the extracellular end of S5 in Shaker (41) that is not present in hERG (Fig. 3).

In a previous study of the binding of hERG activators to the intracellular end of S5, it was noted that W563A, L559A, F557A, and F551A either were not expressed or were expressed only poorly (47). Additionally, L559H has been identified as a Long QT syndrome mutation. These data are all consistent with our findings that these residues are important for hERG function. In addition to the residues in the central section of hERG S5, all of the residues in the S4-S5 linker affected steady state activation. This latter result is expected, given the known role that the S4-S5 linker plays in coupling the voltage sensor domain to the activation gate on S6 (8, 44, 45).

Effect of S5 Mutations on Steady State Inactivation—Residues that affected steady state inactivation were distributed throughout the S5 domain and predominantly lined up on one face of the S5 helix (Leu^{550}, Leu^{553}, Phe^{557}, Ile^{560}, and Leu^{564} along with Trp^{568} and Ile^{571}, residues that when mutated to alanine did not express but when mutated to more conservative residues affected steady state inactivation). This suggests that much of S5 may undergo a reorientation relative to other protein domains, most likely S6, during inactivation. It has been suggested that the S6 domain rotates during inactivation and that this rotation facilitates drug binding (48). Our data are consistent with this hypothesis; however, we cannot determine from our data whether it is only S6 that moves or whether both S5 and S6 move during inactivation.

Three of the residues in the intracellular half of S5 that affect steady state inactivation Leu^{550}, Leu^{553}, and Phe^{557} are also the three residues that when mutated have the greatest impact on binding of the hERG activator RPR260243 (47). One of the major effects of RPR260243 is to shift the voltage dependence of inactivation, a finding that is consistent with our data showing that Leu^{550}, Leu^{553}, and Phe^{557} are important for hERG inactivation.

Whether inactivation in hERG channels is coupled to activation is unresolved (49). The discordance between residues that affect steady state activation and inactivation in this study is more consistent with the view that the two processes are not closely coupled. The clearest example of this discordance is that the mutations that had the largest impact on inactivation, L564A, and activation, W563A, are to adjacent residues, yet neither has a significant impact on the other gating process. Conversely, mutations to residues at the bottom end of S5 (Leu^{550}–Leu^{553}) and to Phe^{557} all resulted in significant perturbations to both steady state activation and inactivation. One interpretation of these data would be that if activation and inactivation are loosely coupled, then it could be via interactions between the voltage sensor and the lower end of S5. This hypothesis however will require further study.

Homology Model of hERG Pore Domain—Because of the importance of drug binding to the pore region of hERG channels, there has been considerable interest in constructing homology models of hERG based on crystal structures of KcsA (50) and KvAP (37). In most of these studies it has been noted that it is very difficult to align S5, *e.g.* Stansfeld *et al.* (50) left S5 out of their model because they were not at all confident of any alignments. Inclusion of S5 helices into pore molecular dynamics simulations is important, because the stability of the structure is dependent upon interactions between the pore, S6, and S5 helices that make up each monomer. We chose the model from Guy and co-workers (37) as a starting point for our work because it contains S5. Small modifications to this model enabled us to generate a plausible explanation for all the mutagenesis data. First, we constrained the model so that inactivation sensitive mutants point in toward S6 (Fig. 5*A*). This also resulted in activation mutants facing outwards, toward the VSD. This latter observation is at odds with the mapping of activation mutants onto a homology model of Shaker (41) where the majority of the activation mutants faced inwards. As noted above, however, there are numerous dissimilarities between the activation properties of hERG and Shaker, and so this difference between our homology model and that of Shaker (41) is perhaps not surprising. More importantly, we obtain similar results with Shaker where the residues with nonfunctioning mutants participate in a tightly packed hydrophobic pocket between the top of S5, the pore helix, and the top of S6 (41). This agreement is highly relevant, considering that the similarity in fold and high pore helix homology across potassium channels with known structures indicate an importance of this region in structural stability.

The molecular mechanisms controlling C-type inactivation have been best characterized in the bacterial KcsA K^+ channel (7, 11) where a hydrogen bond network involving residues Glu^{71} and Asp^{80} is critically involved. A second hydrogen bond network involving residues Trp^{67}, Trp^{68}, and Tyr^{78} is also thought to stabilize the selectivity filter in KcsA (10). None of these residues are conserved in hERG, although it is possible that the hERG equivalents to Glu^{71} and Asp^{80} in KcsA (S620 and N629) could be involved in a hydrogen bond network with a bridging water molecule (7). Alternatively, the presence of tight hydrophobic packing between the top of S5 and the pore helix (Fig. 5*C*) may compensate for the weaker hydrogen bond network in hERG.

In addition to changes in the selectivity filter, there is evidence to suggest that rotation of the inner and/or outer pore domain helices are important components of hERG inactivation. First, Chen *et al.* (48) showed that rotation of the inner helix facilitates high affinity drug binding, which is preferentially associated with the inactivated state (51). Second, here we have shown that mutations to every third or fourth residue in the entire S5 domain perturb inactivation, suggesting that the entire S5 domain experiences a change in environment during channel inactivation. In our homology model we have these residues facing S6. However, whether S5 and S6 both move or just S6, as suggested in previous studies (48), remains to be determined.

Acknowledgments—We thank Tadeusz Marciniec and Ken Wyse for expert technical assistance, Adam Hill, Cath Clarke, Stefan Mann, and Mark Perrin for valuable discussions, and Mark Handschumacher for the initial suggestion of using the "paint roller" concept for representing helices.

REFERENCES

1. Yellen, G. (2002) *Nature* **419,** 35–42
2. Ashcroft, F. M. (2001) *Ion Channels and Disease*, Academic Press, Orlando, FL
3. Curran, M. E., Splawski, I., Timothy, K. W., Vincent, G. M., Green, E. D., and Keating, M. T. (1995) *Cell* **80,** 795–803
4. Sanguinetti, M. C., and Tristani-Firouzi, M. (2006) *Nature* **440,** 463–469
5. Roden, D. M. (2004) *N. Engl. J. Med.* **350,** 1013–1022
6. Vandenberg, J. I., Walker, B. D., and Campbell, T. J. (2001) *Trends Pharmacol. Sci.* **22,** 240–246
7. Cordero-Morales, J. F., Jogini, V., Lewis, A., Vasquez, V., Cortes, D. M., Roux, B., and Perozo, E. (2007) *Nat. Struct. Mol. Biol.* **14,** 1062–1069
8. Long, S. B., Tao, X., Campbell, E. B., and MacKinnon, R. (2007) *Nature* **450,** 376–382
9. Tombola, F., Pathak, M. M., Gorostiza, P., and Isacoff, E. Y. (2007) *Nature* **445,** 546–549
10. Doyle, D. A., Morais Cabral, J., Pfuetzner, R. A., Kuo, A., Gulbis, J. M., Cohen, S. L., Chait, B. T., and MacKinnon, R. (1998) *Science* **280,** 69–77
11. Cordero-Morales, J. F., Cuello, L. G., Zhao, Y., Jogini, V., Cortes, D. M., Roux, B., and Perozo, E. (2006) *Nat. Struct. Mol. Biol.* **13,** 311–318
12. Gao, L., Mi, X., Paajanen, V., Wang, K., and Fan, Z. (2005) *Proc. Natl. Acad. Sci. U. S. A.* **102,** 17630–17635
13. Baukrowitz, T., and Yellen, G. (1995) *Neuron* **15,** 951–960
14. Smith, P. L., Baukrowitz, T., and Yellen, G. (1996) *Nature* **379,** 833–836
15. Spector, P. S., Curran, M. E., Zou, A., Keating, M. T., and Sanguinetti, M. C. (1996) *J. Gen. Physiol.* **107,** 611–619
16. Trudeau, M. C., Warmke, J. W., Ganetzky, B., and Robertson, G. A. (1995) *Science* **269,** 92–95
17. Thompson, J. D., Higgins, D. G., and Gibson, T. J. (1994) *Nucleic Acids Res.* **22,** 4673–4680
18. Riek, R. P., Handschumacher, M. D., Sung, S. S., Tan, M., Glynias, M. J., Schluchter, M. D., Novotny, J., and Graham, R. M. (1995) *J. Theor. Biol.* **172,** 245–258
19. Engelman, D. M., Steitz, T. A., and Goldman, A. (1986) *Annu. Rev. Biophys. Biophys. Chem.* **15,** 321–353
20. Hessa, T., Kim, H., Bihlmaier, K., Lundin, C., Boekel, J., Andersson, H., Nilsson, I., White, S. H., and von Heijne, G. (2005) *Nature* **433,** 377–381
21. Torres, A. M., Bansal, P. S., Sunde, M., Clarke, C. E., Bursill, J. A., Smith, D. J., Bauskin, A., Breit, S. N., Campbell, T. J., Alewood, P. F., Kuchel, P. W., and Vandenberg, J. I. (2003) *J. Biol. Chem.* **278,** 42136–42148
22. Schnolzer, M., Alewood, P., Jones, A., Alewood, D., and Kent, S. B. (1992) *Int. J. Pept. Protein Res.* **40,** 180–193
23. Bax, A., and Davis, D. G. (1985) *J. Magn. Reson.* **65,** 355–360
24. Kumar, A., Ernst, R. R., and Wuthrich, K. (1980) *Biochem. Biophys. Res. Commun.* **95,** 1–6
25. Marion, D., and Wuthrich, K. (1983) *Biochem. Biophys. Res. Commun.* **113,** 967–974
26. Piotto, M., Saudek, V., and Sklenar, V. (1992) *J. Biomol. NMR* **2,** 661–665
27. Bartels, C., Xia, T. H., Billeter, M., Guntert, P., and Wuthrich, K. (1995) *J. Biomol. NMR* **6,** 1–10
28. Clarke, C. E., Hill, A. P., Zhao, J., Kondo, M., Subbiah, R. N., Campbell, T. J., and Vandenberg, J. I. (2006) *J. Physiol.* **573,** 291–304
29. Mitrovic, A. D., Amara, S. G., Johnston, G. A., and Vandenberg, R. J. (1998) *J. Biol. Chem.* **273,** 14698–14706
30. Vandenberg, J. I., Varghese, A., Lu, Y., Bursill, J. A., Mahaut-Smith, M. P., and Huang, C. L. (2006) *Am. J. Physiol.* **291,** C165–C175
31. Li-Smerin, Y., Hackos, D. H., and Swartz, K. J. (2000) *Neuron* **25,** 411–423
32. Piper, D. R., Hinz, W. A., Tallurri, C. K., Sanguinetti, M. C., and Tristani-Firouzi, M. (2005) *J. Biol. Chem.* **280,** 7206–7217
33. Humphrey, W., Dalke, A., and Schulten, K. (1996) *J. Mol. Graph.* **14,** 33–38
34. Phillips, J. C., Braun, R., Wang, W., Gumbart, J., Tajkhorshid, E., Villa, E., Chipot, C., Skeel, R. D., Kale, L., and Schulten, K. (2005) *J. Comput. Chem.* **26,** 1781–1802
35. Mackerell, A. D., Jr., Bashford, D., Bellott, M., Dunbrack, R. L., Jr., Evanseck, J. D., Field, M. J., Fisher, S., Gao, J., Guo, H., Ha, S., Joseph-McCarthy, D., Kuchnir, L., Kuczera, K., Lau, F. T. K., Mattos, C., Michnick, S., Ngo, T., Nguyen, D. T., Prodhom, B., Reiher, W. E., III, Roux, B., Schlenkrich, M., Smith, J. C., Stote, R., Straub, J., Watanabe, M., Wiorkiewicz-Kuczera, J., Yin, D., and M., K. (1998) *J. Phys. Chem. B* **102,** 3586–3616
36. Mackerell, A. D., Jr., Feig, M., and Brooks, C. L., 3rd (2004) *J. Comput. Chem.* **25,** 1400–1415
37. Tseng, G. N., Sonawane, K. D., Korolkova, Y. V., Zhang, M., Liu, J., Grishin, E. V., and Guy, H. R. (2007) *Biophys. J.* **92,** 3524–3540
38. Jiang, Y., Lee, A., Chen, J., Cadene, M., Chait, B. T., and MacKinnon, R. (2002) *Nature* **417,** 523–526
39. Pintacuda, G., and Otting, G. (2002) *J. Am. Chem. Soc.* **124,** 372–373
40. Zangger, K., Gossler, R., Khatai, L., Lohner, K., and Jilek, A. (2008) *Toxicon* **52,** 246–254
41. Soler-Llavina, G. J., Chang, T. H., and Swartz, K. J. (2006) *Neuron* **52,** 623–634
42. Chakrapani, S., Cuello, L. G., Cortes, D. M., and Perozo, E. (2008) *Structure* **16,** 398–409
43. Schneider, R., Ader, C., Lange, A., Giller, K., Hornig, S., Pongs, O., Becker, S., and Baldus, M. (2008) *J. Am. Chem. Soc.* **130,** 7427–7435
44. Ferrer, T., Rupp, J., Piper, D. R., and Tristani-Firouzi, M. (2006) *J. Biol. Chem.* **281,** 12858–12864
45. Long, S. B., Campbell, E. B., and Mackinnon, R. (2005) *Science* **309,** 897–903
46. Yifrach, O., and MacKinnon, R. (2002) *Cell* **111,** 231–239
47. Perry, M., Sachse, F. B., and Sanguinetti, M. C. (2007) *Proc. Natl. Acad. Sci. U. S. A.* **104,** 13827–13832
48. Chen, J., Seebohm, G., and Sanguinetti, M. C. (2002) *Proc. Natl. Acad. Sci. U. S. A.* **99,** 12461–12466
49. Vandenberg, J. I., Torres, A. M., Campbell, T. J., and Kuchel, P. W. (2004) *Eur. Biophys. J.* **33,** 89–97
50. Stansfeld, P. J., Gedeck, P., Gosling, M., Cox, B., Mitcheson, J. S., and Sutcliffe, M. J. (2007) *Proteins* **68,** 568–580
51. Perrin, M. J., Kuchel, P. W., Campbell, T. J., and Vandenberg, J. I. (2008) *Mol. Pharmacol.* **74,** 1443–1452

Figure S1: Table of sequence alignments for the VGK channel superfamily

The header indicates that the alignment os for transmembrane region 5 (TMBR5). The alignment contains 676 sequences in 115 groups. Individual sequences were classified in the same group if for the transmembrane regions the sequences were >95% identical. The colour coding indicates the degree of conservation for residues indicaterd in the table and the helical net diagram shown to the right. The percentage conservation is represented as a number out of 1000, e.g. if a residue is present in 56.4% of sequences then it would be shown as 564. The first column shows the sequence number for the reference sequence, in this case hERG (Genbank: Q12089). The second column shows the position number in the alignment starting at the N-terminal end (which in this case is also the intracellular end). The remainder of the top row lists the 20 amino acids following the GES hydrophobicity scale with the most hydrophobic residue (Phe) at the left-most position. The values shown in the table are normalised to the equivalent of 1000 sequences where 1000 indicates that specific amino acid is conseved 100%. For example, the row corresponding to position 28 is residue 568 in the reference sequence. At this position there is a Phe in 9.2% of sequences, Trp in 14.8%, Thr in 0.9%, Tyr in 63.9%, His in 3.4% and Gln in 7.8%. The boxed residue highlights the residue in the reference sequence, in this case Trp. Also, the Tyr is highlighted in orange indicating that the sequence is conserved in 60-69.9% of sequences. The right hand panel shows the same information as that shown in Figure 1C in the main text and in essence shows a visual representation of the information shown in the Table.

Figure S2: Table of sequence alignments for families within the VGK channel superfamily

A. canonical VGK family; reference sequence is rat Kv12 (Genbank: NP_775118)

B. CNG+HCN families; reference sequence is mouse HCN2 (Genbank: NP_032252)

C. EAG family; reference sequence is hERG (Genbank: Q12809)

Figure S1

TMBR5 of Potassium Channel sequences 676 Sequences in alignment file

Number of sequences scanned: 676. Number of sequence groups: 115 Normalized to 1000.

Residue conservation: 100 | 90.0–>99.9 | 80.0–>89.9 | 70.0–>79.9 | 60.0–>69.9 | 50.0–>59.9 | 30.0–>49.9

Seq#		Psn#	F	M	I	L	V	C	W	A	T	G	Y	S	P	H	Q	N	E	K	D	R
586		46:	246	1	52	70	16	7	137	9	64	89	8	49	17	1	9	156	17	1	41	9
585		45:	10	4	70	61	1	17	63	220	14	57	1	133	104	60	5	35	23	13	85	22
584		44:	17	17	67	19	41	24	25	142	5	62	148	87	46	39	19	23	56	10	153	0
583		43:	43	1	81	23	236	10	24	28	53	3	12	86	320	9	9	22	9	5	25	1
582		42:	19	0	323	14	20	0	254	64	12	34	26	66	25	2	2	17	30	52	30	9
581		41:	35	0	18	12	3	52	0	35	118	30	35	404	21	29	31	41	23	32	33	47
580		40:	36	0	24	19	24	0	0	8	241	11	1	119	64	9	42	68	41	66	203	24
579		39:	291	17	17	85	7	0	0	35	57	28	0	155	34	2	30	57	72	13	82	20
578		38:	49	12	3	42	11	0	4	30	31	192	65	64	83	70	53	66	31	87	88	17
577	*	37:	157	2	64	73	13	0	0	1	172	25	17	189	120	14	4	9	87	21	28	2
576	*	36:	9	10	26	17	25	0	0	78	42	257	4	31	10	0	35	60	126	40	149	81
575	*	35:	0	1	76	22	22	0	0	107	14	43	2	39	123	28	128	77	229	29	46	14
574	*	34:	35	44	7	89	104	0	17	64	21	43	103	104	0	30	10	27	197	21	65	18
573	*	33:	27	54	51	15	57	0	9	22	10	72	9	52	0	9	17	58	158	79	275	26
572	*	32:	0	0	9	17	27	0	0	130	0	139	22	195	70	32	35	23	10	197	0	95
571	*	31:	19	0	224	36	78	0	0	51	0	11	9	0	0	0	0	0	565	0	9	0
570	*	30:	0	9	46	88	143	0	34	593	9	0	9	61	0	0	0	0	0	9	0	0
569	*	29:	361	9	0	108	13	0	0	9	29	0	425	29	0	17	0	0	0	0	0	0
568	*	28:	92	0	0	0	0	0	148	0	9	0	639	0	0	34	78	0	0	0	0	0
567	*	27:	9	62	305	174	371	0	0	45	0	8	0	10	0	0	0	0	17	0	0	0
566	*	26:	17	68	4	226	70	423	0	172	0	9	0	10	0	0	0	0	0	0	0	0
565	*	25:	52	0	0	0	26	0	0	355	152	86	9	267	52	0	0	0	0	0	0	0
564	*	24:	0	29	0	110	9	0	0	167	9	17	0	407	0	0	0	217	0	0	35	0
563	*	23:	486	0	29	46	2	18	330	35	0	0	18	35	0	0	0	0	0	0	0	0
562	*	22:	44	1	211	262	34	0	9	1	18	0	0	1	0	417	0	0	0	0	0	0
561	*	21:	46	41	370	134	78	35	0	191	17	17	0	70	0	0	0	0	0	0	0	0
560	*	20:	0	61	398	176	282	9	0	51	11	0	0	12	0	0	0	0	0	0	0	0
559	*	19:	43	9	53	217	69	17	0	117	17	385	53	20	0	0	0	0	0	0	0	0
558	*	18:	35	111	223	348	148	0	0	83	13	35	0	4	0	0	0	0	0	0	0	0
557	*	17:	327	96	103	115	36	67	0	120	47	11	9	69	0	0	0	0	0	0	0	0
556	*	16:	9	73	54	454	78	4	9	9	53	61	183	14	0	0	0	0	0	0	0	0
555	*	15:	452	35	80	81	0	92	0	40	18	75	26	83	0	17	0	0	0	0	0	0
554	*	14:	256	148	132	213	129	0	0	9	51	1	61	2	0	0	0	0	0	0	0	0
553	*	13:	23	41	260	482	46	0	43	9	87	0	0	0	9	0	0	0	0	0	0	0
552	*	12:	0	0	9	652	9	0	0	52	26	0	0	0	0	17	0	104	0	43	0	87
551	*	11:	107	43	75	416	93	55	0	36	123	26	0	26	0	0	0	0	0	0	0	0
550	*	10:	9	1	239	191	100	35	0	12	25	380	0	9	0	0	0	0	0	0	0	0
549	*	9:	113	17	17	361	213	0	0	0	0	1	0	9	0	0	0	0	0	0	0	269
548	*	8:	94	38	66	10	53	0	35	104	0	0	25	9	0	0	22	0	543	0	0	0
547	*	7:	12	24	107	10	74	9	0	174	26	9	0	50	0	34	49	75	26	89	0	233
546	*	6:	25	153	2	30	26	0	0	152	79	104	195	96	0	17	9	96	0	0	0	17
545	*	5:	0	0	0	0	0	143	0	60	17	0	129	428	139	74	0	9	0	0	0	0
544	*	4:	1	0	9	0	0	0	0	365	9	0	111	75	0	43	83	39	122	42	0	101
543	*	3:	9	17	11	68	26	9	0	79	34	9	43	137	1	11	34	62	0	222	8	220
542		2:	43	55	43	434	76	0	0	9	105	0	148	9	0	0	0	35	9	0	35	0
541		1:	9	17	49	43	62	1	1	35	504	0	35	9	0	44	0	0	0	9	0	183
Seq#		Psn#	F	M	I	L	V	C	W	A	T	G	Y	S	P	H	Q	N	E	K	D	R

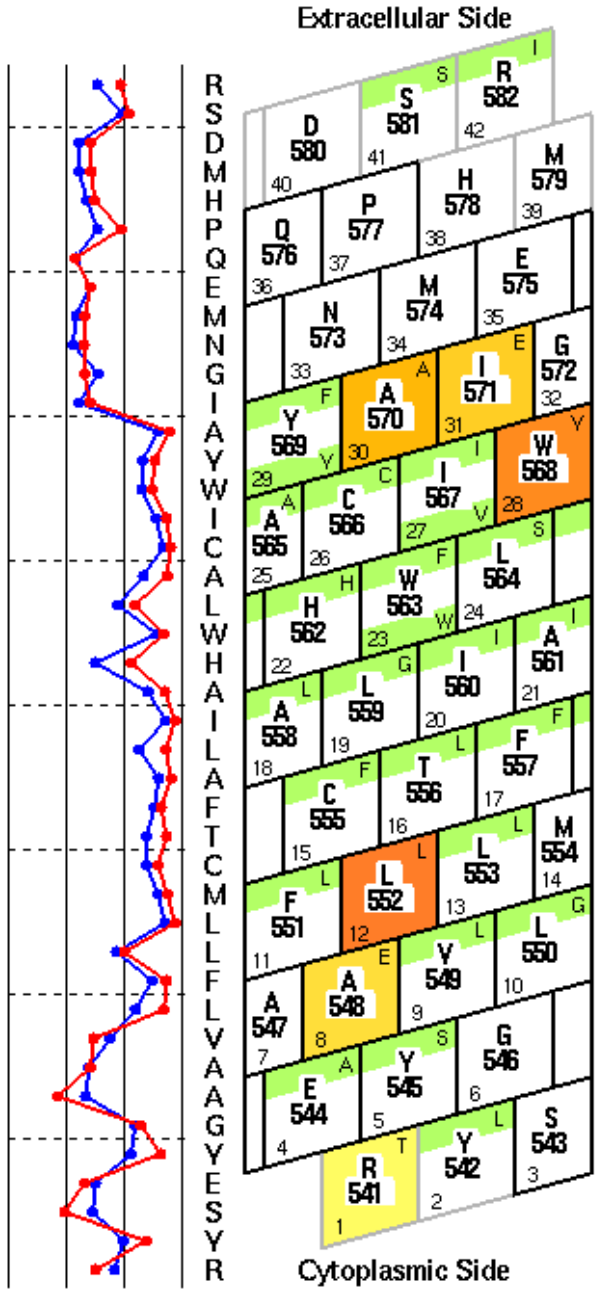

Figure S2a

TMBR5 of Potassium Channel sequences

Number of sequences scanned: 438. Number of sequence groups: 66 Normalized to 1000.

Residue conservation: 100 90.0-->99.9 80.0-->89.9 70.0-->79.9 60.0-->69.9 50.0-->59.9 30.0-->49.9

Seq#		Psn#	F	M	I	L	V	C	W	A	T	G	Y	S	P	H	Q	N	E	K	D	R
363		46:	429	0	45	14	17	13	218	0	91	0	13	80	30	2	0	0	30	0	15	0
362		45:	17	0	15	74	0	30	30	369	8	92	0	197	45	74	0	15	0	15	15	2
361		44:	0	15	72	0	19	42	2	216	6	27	0	93	62	37	33	25	76	17	257	0
360		43:	53	0	51	3	11	17	0	30	30	2	6	119	558	15	15	30	15	0	44	0
359		42:	15	0	544	0	34	0	0	112	2	42	1	108	44	0	2	9	22	19	45	2
358		41:	61	0	32	9	3	1	0	0	87	30	44	579	17	17	22	34	2	12	15	35
357		40:	62	0	18	0	21	0	0	0	336	19	1	158	103	16	58	66	20	80	31	11
356		39:	499	0	15	76	0	0	0	47	20	34	1	54	0	0	15	52	48	2	124	15
355		38:	85	18	0	57	15	0	0	22	46	29	45	55	24	96	91	103	51	152	99	14
354	*	37:	2	4	4	0	23	0	0	2	298	44	15	307	121	20	5	0	83	36	33	4
353	*	36:	16	0	0	15	13	0	0	105	44	98	0	53	17	0	45	100	190	64	199	41
352	*	35:	0	0	19	1	23	0	0	186	25	60	4	67	214	48	18	119	74	50	65	25
351	*	34:	17	25	12	56	120	0	0	40	35	76	0	108	1	37	15	17	320	0	113	8
350	*	33:	0	15	89	15	30	0	15	0	17	125	1	29	0	0	15	5	237	2	404	0
349	*	32:	0	0	15	15	47	0	0	196	0	15	23	22	0	41	61	40	17	343	0	165
348	*	31:	0	0	0	0	0	0	0	0	0	1	0	0	0	0	0	0	984	0	15	0
347	*	30:	0	15	44	15	133	0	15	763	15	0	0	0	0	0	0	0	0	0	0	0
346	*	29:	362	15	0	173	23	0	0	15	51	0	312	49	0	0	0	0	0	0	0	0
345	*	28:	138	0	0	0	0	0	0	0	0	0	787	0	0	60	15	0	0	0	0	0
344	*	27:	15	97	186	15	573	0	0	58	0	14	0	12	0	0	0	0	30	0	0	0
343	*	26:	30	119	7	394	121	15	0	280	1	15	0	17	0	0	0	0	0	0	0	0
342	*	25:	91	0	0	0	45	1	0	101	235	14	15	407	91	0	0	0	0	0	0	0
341	*	24:	0	0	0	0	0	0	0	276	0	30	0	694	0	0	0	0	0	0	0	0
340	*	23:	847	0	0	0	0	0	0	61	0	0	31	61	0	0	0	0	0	0	0	0
339	*	22:	77	3	368	457	59	0	0	1	32	0	0	3	0	0	0	0	0	0	0	0
338	*	21:	51	41	418	143	120	0	0	76	30	0	0	121	0	0	0	0	0	0	0	0
337	*	20:	0	45	391	121	427	0	0	0	15	0	0	0	0	0	0	0	0	0	0	0
336	*	19:	0	15	0	0	30	30	0	205	15	670	0	34	0	0	0	0	0	0	0	0
335	*	18:	0	163	335	258	245	0	0	0	0	0	0	0	0	0	0	0	0	0	0	0
334	*	17:	312	0	45	64	33	117	0	209	81	19	0	120	0	0	0	0	0	0	0	0
333	*	16:	0	19	67	776	32	0	0	0	0	106	0	0	0	0	0	0	0	0	0	0
332	*	15:	750	0	106	15	0	0	0	0	0	0	45	83	0	0	0	0	0	0	0	0
331	*	14:	446	16	91	311	30	0	0	0	0	0	106	0	0	0	0	0	0	0	0	0
330	*	13:	25	56	452	295	65	0	76	15	0	0	0	0	15	0	0	0	0	0	0	0
329	*	12:	0	0	0	879	15	0	0	76	30	0	0	0	0	0	0	0	0	0	0	0
328	*	11:	83	45	30	697	0	38	0	0	106	0	0	0	0	0	0	0	0	0	0	0
327	*	10:	15	2	112	76	39	61	0	21	13	663	0	0	0	0	0	0	0	0	0	0
326	*	9:	197	15	0	628	160	0	0	0	0	0	0	0	0	0	0	0	0	0	0	0
325	*	8:	0	0	0	0	0	0	0	0	0	0	0	15	0	0	38	0	946	0	1	0
324	*	7:	0	0	0	0	0	15	0	0	30	0	0	87	0	59	86	131	45	140	0	406
323	*	6:	43	266	4	50	30	0	0	158	122	0	189	91	0	0	15	0	0	0	0	30
322	*	5:	0	0	0	0	0	240	0	0	0	0	0	654	0	106	0	0	0	0	0	0
321	*	4:	0	0	15	0	0	0	0	545	16	0	13	101	0	61	68	20	0	0	0	160
320	*	3:	15	15	0	1	0	15	0	17	29	0	76	0	0	19	60	0	0	370	0	383
319		2:	61	34	59	698	133	0	0	15	0	0	0	0	0	0	0	0	0	0	0	0
318		1:	0	0	0	0	76	0	0	45	878	0	0	1	0	0	0	0	0	0	0	0
Seq#		Psn#	F	M	I	L	V	C	W	A	T	G	Y	S	P	H	Q	N	E	K	D	R

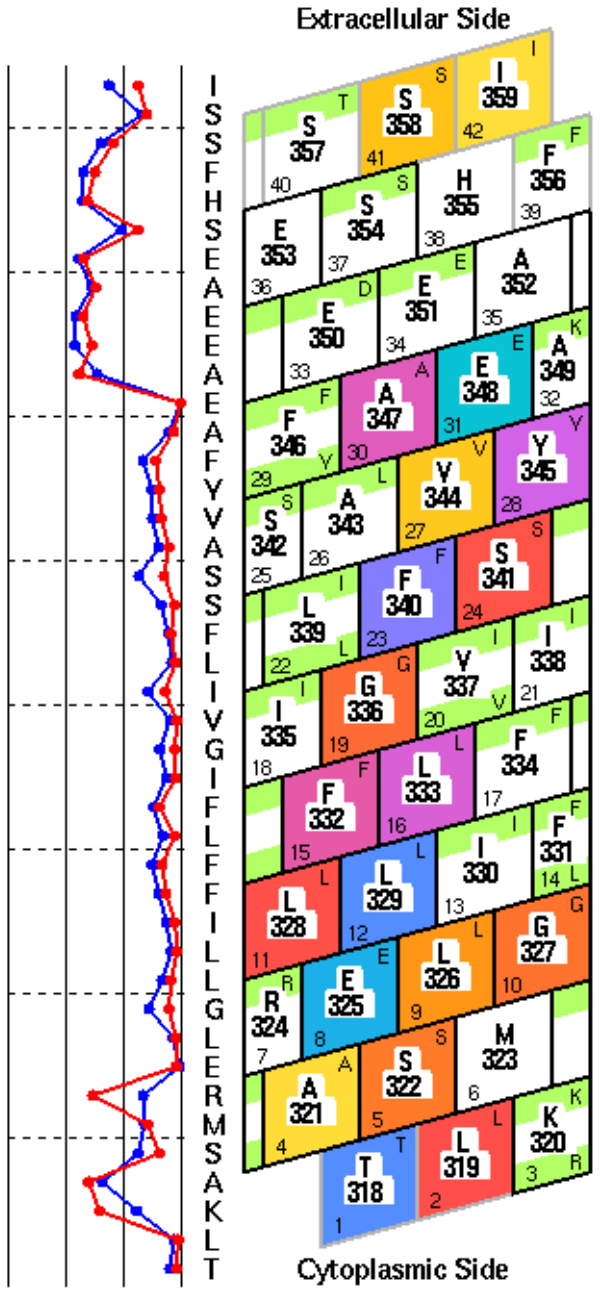

Figure S2b

TMBR5 of Potassium Channel sequences

Number of sequences scanned: 123. Number of sequence groups: 28 Normalized to 1000.

Residue conservation: 100 90.0–>99.9 80.0–>89.9 70.0–>79.9 60.0–>69.9 50.0–>59.9 30.0–>49.9

Seq#		Psn#	F	M	I	L	V	C	W	A	T	G	Y	S	P	H	Q	N	E	K	D	R
336		46:	0	0	18	18	0	0	0	36	0	255	0	5	0	0	0	502	0	0	131	36
335		45:	0	10	215	41	0	0	0	0	0	0	0	71	321	36	0	50	36	15	200	5
334		44:	0	0	36	0	71	0	0	72	5	0	607	137	0	36	0	36	0	0	0	0
333		43:	36	0	0	0	857	0	0	0	71	0	36	0	0	0	0	0	0	0	0	0
332		42:	7	0	0	0	0	0	957	0	0	0	36	0	0	0	0	0	0	0	0	0
331		41:	0	0	0	0	5	214	0	61	138	0	0	202	2	26	36	54	71	92	36	62
330		40:	0	0	0	36	0	0	0	0	179	0	0	71	0	0	36	45	0	0	562	71
329		39:	0	0	36	36	27	0	0	21	180	0	0	403	136	10	0	21	41	0	46	45
328		38:	0	0	0	0	0	0	0	36	0	607	36	36	286	0	0	0	0	0	0	0
327	*	37:	571	0	113	244	0	0	0	0	0	0	36	0	0	0	0	36	0	0	0	0
326	*	36:	0	0	0	0	0	0	0	0	71	714	0	0	0	0	0	0	71	0	143	0
325	*	35:	0	2	265	89	36	0	0	0	0	36	0	0	0	0	412	36	123	0	0	0
324	*	34:	105	0	0	214	47	0	0	54	3	0	279	137	0	36	0	71	54	0	0	0
323	*	33:	71	188	0	27	143	0	0	32	0	0	36	71	0	0	0	18	36	286	57	36
322	*	32:	0	0	0	0	0	0	0	0	0	0	36	643	286	36	0	0	0	0	0	0
321	*	31:	43	0	276	110	321	0	0	208	0	42	0	0	0	0	0	0	0	0	0	0
320	*	30:	0	0	71	325	146	0	104	247	0	0	0	107	0	0	0	0	0	0	0	0
319	*	29:	585	0	0	36	0	0	0	0	0	0	305	4	0	71	0	0	0	0	0	0
318	*	28:	52	0	0	0	0	0	0	0	36	0	626	0	0	0	286	0	0	0	0	0
317	*	27:	0	24	266	633	77	0	0	0	0	0	0	0	0	0	0	0	0	0	0	0
316	*	26:	0	0	0	0	0	964	0	36	0	0	0	0	0	0	0	0	0	0	0	0
315	*	25:	0	0	0	0	0	0	0	542	36	321	0	101	0	0	0	0	0	0	0	0
314	*	24:	0	0	0	0	0	0	0	36	0	0	0	36	0	0	0	786	0	0	143	0
313	*	23:	0	0	71	130	10	39	750	0	0	0	0	0	0	0	0	0	0	0	0	0
312	*	22:	0	0	0	0	0	0	36	0	0	0	0	0	0	964	0	0	0	0	0	0
311	*	21:	71	71	393	214	36	143	0	0	0	71	0	0	0	0	0	0	0	0	0	0
310	*	20:	0	71	407	293	39	36	0	107	11	0	0	36	0	0	0	0	0	0	0	0
309	*	19:	175	0	216	286	213	0	0	0	36	0	75	0	0	0	0	0	0	0	0	0
308	*	18:	143	0	79	750	29	0	0	0	0	0	0	0	0	0	0	0	0	0	0	0
307	*	17:	36	286	317	286	71	0	0	0	4	0	0	0	0	0	0	0	0	0	0	0
306	*	16:	0	214	0	36	71	0	36	36	0	0	607	0	0	0	0	0	0	0	0	0
305	*	15:	71	71	77	245	0	60	0	32	39	295	0	38	0	71	0	0	0	0	0	0
304	*	14:	0	107	327	0	314	0	0	36	208	2	0	6	0	0	0	0	0	0	0	0
303	*	13:	36	0	0	679	36	0	0	0	250	0	0	0	0	0	0	0	0	0	0	0
302	*	12:	0	0	36	0	0	0	0	36	36	0	0	0	0	71	0	429	0	143	0	250
301	*	11:	103	5	188	0	214	134	0	102	41	107	0	107	0	0	0	0	0	0	0	0
300	*	10:	0	0	611	0	282	0	0	0	71	0	0	36	0	0	0	0	0	0	0	0
299	*	9:	0	0	0	0	0	0	0	0	0	3	0	36	0	0	0	0	0	0	0	961
298	*	8:	388	71	110	40	143	0	143	0	0	0	104	0	0	0	0	0	0	0	0	0
297	*	7:	36	84	390	40	305	0	0	110	0	0	0	0	0	0	0	0	0	36	0	0
296	*	6:	0	0	0	3	36	0	0	250	0	0	282	36	0	0	0	393	0	0	0	0
295	*	5:	0	0	0	0	0	0	0	211	71	0	0	218	464	0	0	36	0	0	0	0
294	*	4:	5	0	0	0	0	0	0	214	0	0	423	0	0	36	0	39	71	171	0	39
293	*	3:	0	36	0	179	107	3	0	214	71	36	0	61	3	0	0	254	0	3	32	0
292		2:	0	146	0	101	0	0	0	0	432	0	0	0	0	0	0	143	36	0	143	0
291		1:	36	71	201	143	39	3	3	36	0	0	143	0	0	71	0	0	0	0	0	254
Seq#		Psn#	F	M	I	L	V	C	W	A	T	G	Y	S	P	H	Q	N	E	K	D	R

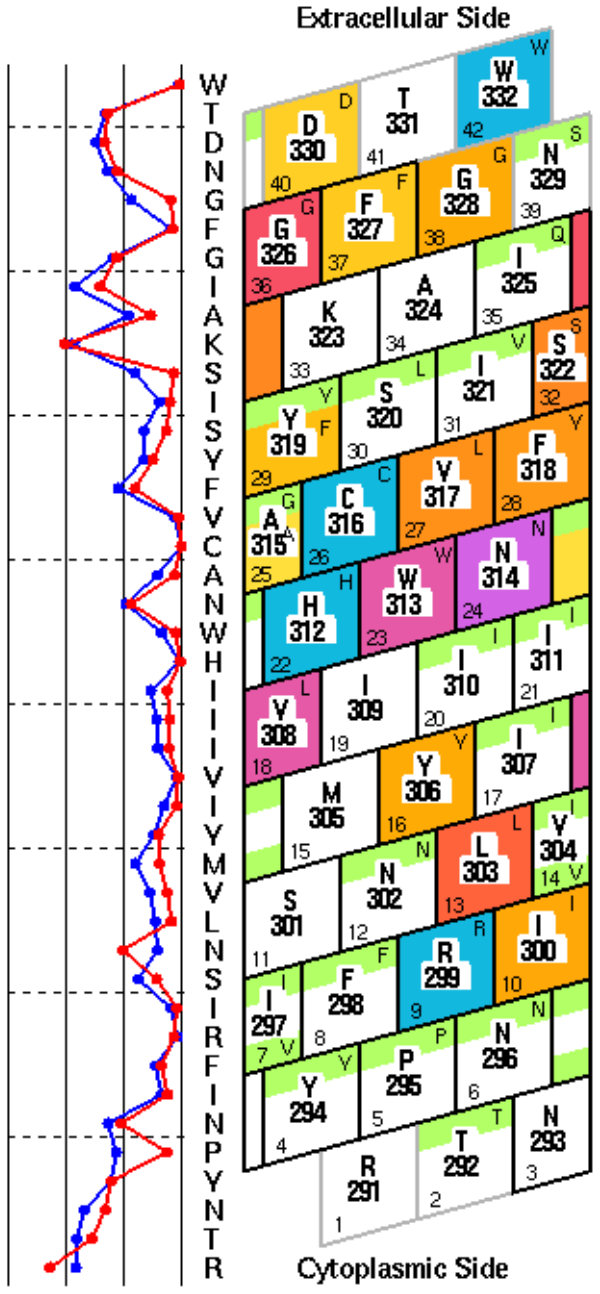

Figure S2c

TMBR5 of Potassium Channel sequences (erg, eag & elk)
Number of sequences scanned: 108. Number of sequence groups: 17 Normalized to 1000.
Residue conservation: 100 90.0–>99.9 80.0–>89.9 70.0–>79.9 60.0–>69.9 50.0–>59.9 30.0–>49.9

Seq#		Psn#	F	M	I	L	V	C	W	A	T	G	Y	S	P	H	Q	N	E	K	D	R
586		46:	0	4	148	391	39	0	80	0	77	44	0	12	0	0	59	133	0	8	5	0
585		45:	0	8	59	59	5	0	308	0	63	29	8	0	0	59	33	0	98	7	126	136
584		44:	0	0	118	125	85	0	162	0	0	316	0	0	67	63	0	0	25	0	39	0
583		43:	0	4	346	120	20	0	166	15	124	17	0	118	0	5	0	29	0	34	0	4
582		42:	0	0	17	96	0	0	83	0	77	70	50	29	0	13	5	83	118	275	29	54
581		41:	0	0	0	44	0	0	0	77	232	87	64	149	74	89	65	0	29	20	44	24
580		40:	0	0	36	67	79	0	0	57	35	0	0	73	29	0	0	16	200	137	269	0
579		39:	29	116	0	221	0	0	0	20	8	59	0	76	5	0	4	147	232	85	0	0
578		38:	0	15	20	65	15	0	29	57	31	9	205	162	0	105	9	50	10	0	214	5
577	*	37:	59	0	118	33	0	0	0	0	8	0	0	87	338	20	9	5	265	0	59	0
576	*	36:	0	69	176	59	123	0	0	59	0	0	29	0	0	0	59	20	0	20	0	387
575	*	35:	0	0	0	0	0	0	0	0	0	0	0	0	0	0	0	0	941	0	59	0
574	*	34:	0	171	0	5	160	0	0	185	0	0	176	59	0	0	8	0	0	145	0	92
573	*	33:	4	0	0	0	29	0	0	0	0	0	0	63	0	59	59	344	88	59	176	118
572	*	32:	0	0	0	0	0	0	0	118	0	882	0	0	0	0	0	0	0	0	0	0
571	*	31:	0	0	1000	0	0	0	0	0	0	0	0	0	0	0	0	0	0	0	0	0
570	*	30:	0	0	22	0	213	0	0	471	0	0	59	235	0	0	0	0	0	0	0	0
569	*	29:	74	0	0	0	0	0	0	0	0	0	926	0	0	0	0	0	0	0	0	0
568	*	28:	0	0	0	0	0	0	1000	0	0	0	0	0	0	0	0	0	0	0	0	0
567	*	27:	0	0	903	0	97	0	0	0	0	0	0	0	0	0	0	0	0	0	0	0
566	*	26:	0	0	0	0	0	1000	0	0	0	0	0	0	0	0	0	0	0	0	0	0
565	*	25:	0	0	0	0	0	0	0	1000	0	0	0	0	0	0	0	0	0	0	0	0
564	*	24:	0	196	0	745	59	0	0	0	0	0	0	0	0	0	0	0	0	0	0	0
563	*	23:	0	0	0	0	0	0	1000	0	0	0	0	0	0	0	0	0	0	0	0	0
562	*	22:	0	0	0	0	0	0	0	0	0	0	0	0	0	1000	0	0	0	0	0	0
561	*	21:	0	0	0	0	0	0	0	1000	0	0	0	0	0	0	0	0	0	0	0	0
560	*	20:	0	0	446	181	188	0	0	165	0	0	0	20	0	0	0	0	0	0	0	0
559	*	19:	0	0	0	1000	0	0	0	0	0	0	0	0	0	0	0	0	0	0	0	0
558	*	18:	0	59	20	0	4	0	0	565	88	235	0	29	0	0	0	0	0	0	0	0
557	*	17:	941	0	0	0	0	0	0	0	0	0	59	0	0	0	0	0	0	0	0	0
556	*	16:	59	66	106	0	287	29	0	0	360	0	0	93	0	0	0	0	0	0	0	0
555	*	15:	29	0	0	88	0	525	0	220	0	20	0	118	0	0	0	0	0	0	0	0
554	*	14:	0	765	0	59	176	0	0	0	0	0	0	0	0	0	0	0	0	0	0	0
553	*	13:	0	0	0	1000	0	0	0	0	0	0	0	0	0	0	0	0	0	0	0	0
552	*	12:	0	0	0	1000	0	0	0	0	0	0	0	0	0	0	0	0	0	0	0	0
551	*	11:	173	106	78	109	235	5	0	0	294	0	0	0	0	0	0	0	0	0	0	0
550	*	10:	0	0	0	1000	0	0	0	0	0	0	0	0	0	0	0	0	0	0	0	0
549	*	9:	0	59	118	0	824	0	0	0	0	0	0	0	0	0	0	0	0	0	0	0
548	*	8:	0	140	49	0	105	0	0	706	0	0	0	0	0	0	0	0	0	0	0	0
547	*	7:	0	5	0	0	0	0	0	937	59	0	0	0	0	0	0	0	0	0	0	0
546	*	6:	0	0	0	0	0	0	0	0	59	706	0	235	0	0	0	0	0	0	0	0
545	*	5:	0	0	0	0	0	37	0	0	0	0	875	0	0	88	0	0	0	0	0	0
544	*	4:	0	0	0	0	0	0	0	0	0	0	0	0	0	0	294	0	706	0	0	0
543	*	3:	0	0	77	158	0	0	0	0	0	0	0	765	0	0	0	0	0	0	0	0
542		2:	0	0	0	0	0	0	0	0	0	0	1000	0	0	0	0	0	0	0	0	0
541		1:	0	0	0	0	0	0	0	0	0	0	0	0	0	181	0	0	0	0	0	819
Seq#		Psn#	F	M	I	L	V	C	W	A	T	G	Y	S	P	H	Q	N	E	K	D	R

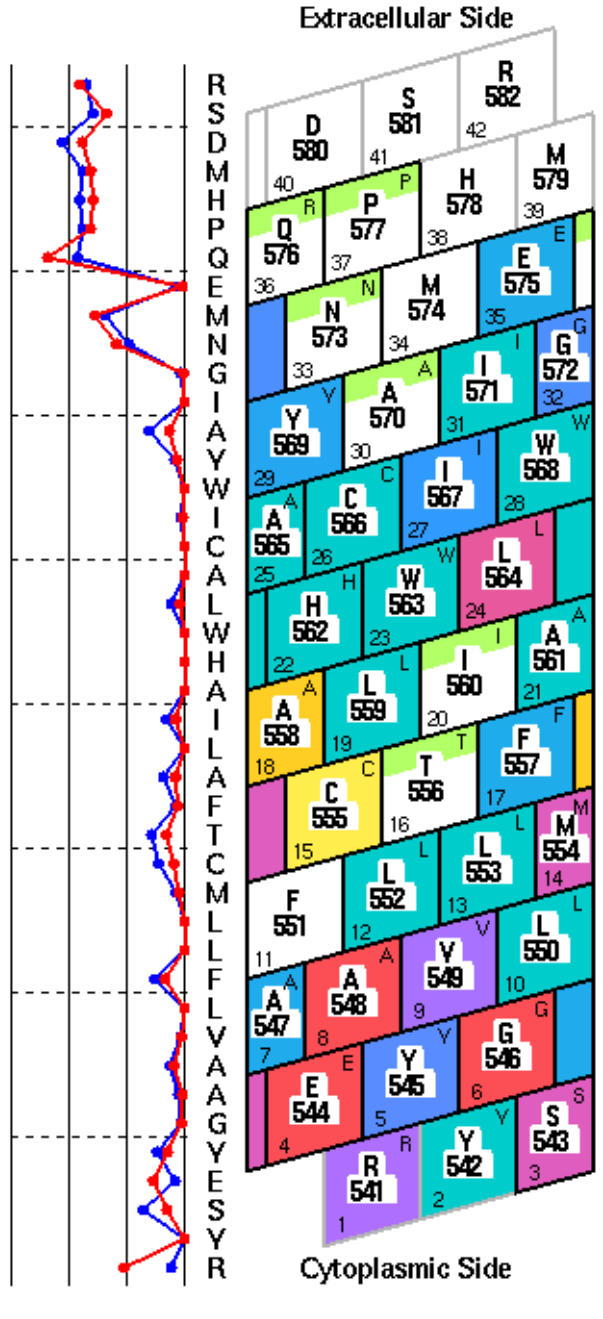

Table S1. Activation parameters for mutant hERG channels.

Construct (n)	$V_{0.5}$	k	ΔG_0	$\Delta\Delta G_0$
	mV	mV	Kcal/mol	Kcal/mol
WT (5)	-23.5 ± 0.5	7.3 ± 0.2	-1.9 ± 0.05	
S543A (5)	-52.7 ± 1.2	7.1 ± 0.4	-4.4 ± 0.3	-2.5 ± 0.4
E544A (5)	-34.7 ± 1.3	5.6 ± 0.1	-3.7 ± 0.2	-1.8 ± 0.3
Y545A (5)	-38.7 ± 0.4	6.4 ± 0.3	-3.6 ± 0.2	-1.7 ± 0.3
G546A (7)	-68.8 ± 1.8	8.7 ± 0.3	-4.4 ± 0.2	-2.5 ± 0.3
A547V (5)	-11.1 ± 1.2	7.6 ± 0.3	-0.9 ± 0.1	1.0 ± 0.2
A548V (4)	-54.0 ± 0.2	7.1 ± 0.1	-4.8 ± 0.1	-2.9 ± 0.2
V549A (4)	-7.9 ± 1.7	8.6 ± 0.4	-0.5 ± 0.1	1.4 ± 0.2
L550A (4)	-41.2 ± 0.7	10.0 ± 0.7	-2.4 ± 0.2	-0.5 ± 0.2
F551A (5)	-37.4 ± 1.3	6.2 ± 0.4	-3.7 ± 0.4	1.8 ± 0.4
L552A (5)	-30.9 ± 0.6	10.8 ± 0.4	-1.7 ± 0.1	0.2 ± 0.2
L553A (3)	-23.6 ± 0.6	7.5 ± 0.3	-1.8 ± 0.1	0.1 ± 0.1
M554A (4)	-35.3 ± 0.4	7.3 ± 0.1	-2.8 ± 0.003	-0.9 ± 0.05
C555A (3)	-22.7 ± 3.3	7.6 ± 0.6	-1.8 ± 0.3	0.1 ± 0.3
T556A (4)	-11.0 ± 1.2	7.9 ± 0.6	-0.9 ± 0.1	1.0 ± 0.2
F557A	NE			
F557L (5)	-29.0 ± 1.5	7.9 ± 0.1	-2.2 ± 0.1	-0.3 ± 0.2
A558V (4)	-29.4 ± 0.8	7.5 ± 0.2	-2.3 ± 0.1	-0.4 ± 0.2
L559A (4)	-48.6 ± 2.1	6.5 ± 0.3	-4.4 ± 0.1	-2.5 ± 0.2
I560A (4)	-18.7 ± 1.5	7.4 ± 0.3	-1.5 ± 0.2	0.4 ± 0.2
A561V	NE			
A561C (4)	-21.3 ± 0.5	6.7 ± 0.2	-1.9 ± 0.1	0.0 ± 0.1
H562A	NE			
H562N	NE			
H562T	NE			
W563A (3)	-54.6 ± 0.9	6.3 ± 0.1	-5.1 ± 0.1	-3.2 ± 0.2
L564A (4)	-34.0 ± 1.0	7.6 ± 0.5	-2.7 ± 0.2	-0.8 ± 0.3
A565V	NE			

A565C (6)	-14.9 ± 1.1	6.6 ± 0.2	-1.2 ± 0.1	0.7 ± 0.1
C566A (3)	-24.9 ± 0.7	6.9 ± 0.2	-2.1 ± 0.1	-0.3 ± 0.2
I567A (4)	-14.4 ± 1.1	7.5 ± 0.4	-1.2 ± 0.1	0.7 ± 0.2
W568A	NE			
W568F (1)*	-25.4	7.0		
Y569A (4)	-13.7 ± 0.5	6.7 ± 0.1	-1.2 ± 0.05	0.7 ± 0.1
A570V (4)	-31.1 ± 0.8	7.5 ± 0.04	-2.4 ± 0.1	-0.5 ± 0.1
I571A	NE			
I571L (4)	-16.2 ± 0.8	6.9 ± 0.2	-1.4 ± 0.1	0.5 ± 0.1
G572A (3)	-20.2 ± 0.7	7.2 ± 0.2	-1.6 ± 0.03	0.2 ± 0.1
N573A (3)	-26.1 ± 0.4	7.4 ± 0.2	-2.1 ± 0.1	-0.2 ± 0.1
M574A (4)	-17.9 ± 0.4	7.8 ± 0.3	-1.3 ± 0.04	0.6 ± 0.1
E575A (5)	-19.0 ± 0.6	7.9 ± 0.2	-1.4 ± 0.1	0.5 ± 0.1
Q576A	NE			
Q576N (4)	-23.3 ± 0.7	7.0 ± 0.1	-1.9 ± 0.1	0.0 ± 0.1
P577A (4)	-28.2 ± 1.2	6.8 ± 0.5	-2.4 ± 0.1	-0.5 ± 0.2

Data are means ± S.E.M. for (n) experiments. $V_{0.5}$ is the voltage for half activation, k is the slope factor. NE: no expression. * Despite repeated injectiojns and preparations of RNA we were only able to obtain one analyzable recording for W568F.

Table S2. Inactivation parameters for mutant hERG channels

Construct (n)	$V_{0.5}$	k	ΔG_0	$\Delta\Delta G_0$	E_{rev}
	mV	mV	Kcal/mol	Kcal/mol	mV
WT (8)	-77.4 ± 0.6	-27.6 ± 1.9	1.6 ± 0.1		-95 ± 0.6
S543A (5)	-62.2 ± 3.2	-21.6 ± 1.3	1.7 ± 0.1	0.1 ± 0.2	-96 ± 0.9
E544A (4)	-59.6 ± 1.1	-26.2 ± 0.7	1.3 ± 0.02	-0.3 ± 0.1	-96 ± 0.1
Y545A (5)	-59.2 ± 2.5	-28.7 ± 1.8	1.2 ± 0.1	-0.4 ± 0.2	-97 ± 0.9
G546A (4)	-60.2 ± 2.7	-23.8 ± 0.5	1.5 ± 0.1	-0.2 ± 0.2	-91 ± 0.1
A547V (3)	-73.0 ± 0.6	-26.1 ± 1.7	1.7 ± 0.1	0.1 ± 0.2	-97 ± 0.6
A548V (4)	-68.4 ± 1.2	-21.8 ± 0.6	1.8 ± 0.1	0.2 ± 0.2	-96 ± 0.3
V549A (3)	-66.5 ± 4.8	-34.0 ± 1.6	1.2 ± 0.1	-0.4 ± 0.2	-97 ± 1.4
L550A (3)	-17.6 ± 3.5	-26.3 ± 0.7	0.4 ± 0.1	-1.3 ± 0.2	-94 ± 0.7
F551A (4)	-46.3 ± 3.4	-32.9 ± 0.4	0.8 ± 0.1	-0.8 ± 0.2	-95 ± 0.3
L552A (3)	-31.8 ± 1.7	-23.8 ± 1.6	0.8 ± 0.02	-0.9 ± 0.1	-98 ± 0.6
L553A (4)	-93.5 ± 2.2	-24.2 ± 1.1	2.3 ± 0.03	0.6 ± 0.1	-98 ± 0.6
M554A (4)	-84.7 ± 1.8	-31.6 ± 1.6	1.6 ± 0.1	0.1 ± 0.2	-95 ± 1.5
C555A (5)	-36.6 ± 2.3	-34.5 ± 1.9	0.6 ± 0.02	-1.0 ± 0.1	-96 ± 1.4
T556A (4)	-66.9 ± 2.4	-28.4 ± 1.7	1.4 ± 0.1	-0.2 ± 0.2	-97 ± 1.3
F557A	NE				
F557L (5)	-113.3 ±1.6	-30.7 ± 0.02	2.2 ± 0.01	0.6 ± 0.1	-97 ± 1.0
A558V (2)	-55.9 ± 0.4	-26.4 ± 2.4	1.3 ± 0.1	-0.3 ± 0.2	-97 ± 0.5
L559A (4)	-91.0 ± 0.4	-25.2 ± 0.5	2.1 ± 0.04	0.5 ± 0.1	-96 ± 0.8
I560A (5)	-43.8 ± 1.2	-31.2 ± 1.1	0.8 ± 0.1	-0.8 ± 0.2	-96 ± 0.9
A561V	NE				
A561C (4)	-66.1 ± 1.1	-26.0 ± 1.0	1.5 ± 0.1	-0.2 ± 0.2	-96 ± 0.2
H562A	NE				
H562N	NE				
H562T	NE				
W563A (4)	-93.8 ± 1.2	-32.7 ± 1.1	1.7 ± 0.1	0.1 ± 0.2	-97 ± 0.9
L564A (4)	-4.9 ± 1.6	-22.0 ± 0.5	0.1 ± 0.04	-1.5 ± 0.1	-97 ± 0.9
A565V	NE				

A565C (4)	-74.3 ± 1.9	-24.6 ± 2.0	1.8 ± 0.2	0.2 ± 0.3	-96 ± 0.2
C566A (4)	-78.1 ± 3.2	-25.9 ± 1.1	1.8 ± 0.1	0.2 ± 0.2	-99 ± 0.1
I567A (4)	-71.2 ± 0.7	-32.4 ± 0.6	1.3 ± 0.03	-0.3 ± 0.1	-98 ± 0.3
W568A	NE				
W568F (1)*	-101.6	-24.9			-92.4
Y569A (3)	-84.9 ± 0.5	-27.8 ± 0.9	1.8 ± 0.1	0.2 ± 0.1	-97 ± 0.4
A570V (4)	-90.5 ± 0.2	-30.2 ± 0.7	1.8 ± 0.04	0.2 ± 0.1	-98 ± 0.2
I571A	NE				
I571L (4)	-94.2 ± 1.2	-29.8 ± 1.0	2.0 ± 0.1	0.4 ± 0.2	-91 ± 0.3
G572A (5)	-93.1 ± 0.4	-27.8 ± 1.1	2.0 ± 0.1	0.3 ± 0.2	-97 ± 0.2
N573A (4)	-48.7 ± 1.6	-31.2 ± 1.4	0.9 ± 0.1	-0.7 ± 0.2	-97 ± 1.5
M574A (4)	-68.3 ± 1.7	-29.1 ± 1.6	1.3 ± 0.1	-0.3 ± 0.2	-95 ± 0.7
E575A (6)	-100.8 ± 1.1	-24.3 ± 1.0	2.5 ± 0.1	0.9 ± 0.2	-98 ± 0.3
Q576A	NE				
Q576N (4)	-86.7 ± 1.2	-26.2 ± 0.8	1.9 ± 0.1	0.3 ± 0.2	-99 ± 0.1
P577A (4)	-14.8 ± 1.1	-27.1 ± 0.7	0.3 ± 0.02	-1.3 ± 0.1	-94 ± 1.6

Data are means ± S.E.M. for (n) experiments. $V_{0.5}$ is the voltage for half inactivation, k is the slope factor and Erev is the reversal potential. NE: no expression. * Despite repeated injectiojns and preparations of RNA we were only able to obtain one analyzable recording for W568F